

**HEAT TRANSFER ENHANCEMENT FOR TURBULENT FLOW  
THROUGH BLOCKAGES WITH ELONGATED HOLES  
IN A RECTANGULAR CHANNEL**

A Thesis

by

YONGHEE LEE

Submitted to the Office of Graduate Studies of  
Texas A&M University  
in partial fulfillment of the requirements for the degree of  
MASTER OF SCIENCE

May 2007

Major Subject: Mechanical Engineering

**HEAT TRANSFER ENHANCEMENT FOR TURBULENT FLOW  
THROUGH BLOCKAGES WITH ELONGATED HOLES  
IN A RECTANGULAR CHANNEL**

A Thesis

by

YONGHEE LEE

Submitted to the Office of Graduate Studies of  
Texas A&M University  
in partial fulfillment of the requirements for the degree of  
MASTER OF SCIENCE

Approved by:

Chair of Committee,	S.C. Lau
Committee Members,	N.K. Anand
	Yassin A. Hassan
Head of Department,	Dennis O'Neal

May 2007

Major Subject: Mechanical Engineering

## ABSTRACT

Heat Transfer Enhancement for Turbulent Flow through Blockages  
with Elongated Holes in a Rectangular Channel. (May 2007)

Yonghee Lee, B.S., Sungkyunkwan University

Chair of Advisory Committee: Dr. S.C. Lau

In this thesis, turbulent forced convective heat transfer downstream of blockages with elongated holes in a rectangular channel was studied.

The rectangular channel has a width-to-height ratio of 12:1. The blockages have the same cross section as that of the channel. The diameter of all elongated holes of the blockages is three quarters of the channel height. The blockages are classified into two different types with two different hole-to-blockage area ratios (ratio of total cross-sectional area of holes to cross-sectional surface area of the blockage) of 0.5 or 0.6. For each hole-to-blockage area ratio, the blockages are again subdivided into three different cases using three different aspect ratios (hole-width-to-height ratio) which are determined by the number of holes – four, six, and eight holes per blockage. Experiments for total six different cases of blockages were performed under a uniform wall temperature condition (50°C). The experiments were conducted at three different Reynolds numbers of about 7,000, 12,000, and 17,000, respectively. Three copper plate heaters with twenty one embedded thermocouples were used to measure the average heat transfer on the surface of channel walls between two consecutive blockages.

Results from this study showed that the blockages with elongated holes enhance the average heat transfer by up to 5.06 and 4.08 times that by fully developed turbulent flow through a smooth channel at the same Reynolds numbers for small and large hole-to-blockage area ratios, respectively. The friction factor ratios for small and large hole-to-blockage area ratios of the blockages reached 345 and 89 times, respectively, that by fully developed turbulent flow through a smooth channel at the same Reynolds numbers. TP (Thermal Performance) values varied from 0.65 to 1.11 depending on cases.

According to the results, Case L-2, which has six elongated holes and hole-to-blockage area ratio of 0.6, is the best option from the TP point of view. But Case S-2, which also had six elongated holes and hole-to-blockage area ratio of 0.5, can be an alternative when more weight should be put on the heat transfer enhancement than TP value.

## DEDICATION

To my father and mother

To my lovely wife, *Youchin*

To my beloved son, *Youchan*

To my dear friends, *Keunmin and Kyuyong*

Most of all to my devoted father-in-law and mother-in-law

## ACKNOWLEDGMENTS

I really appreciate Dr. S.C. Lau for teaching and guiding me as an advisor for my graduate study and thesis research in Texas A&M University. I could learn a lot about experimental convective heat transfer through his assistance and guidance during preparing and advancing my thesis research. From his *conduction and radiation* subject, especially I could enlarge profoundly the range of mathematical and practical understanding about conduction problems. I am sure that academic knowledge and research experience acquired from him will be invaluable for pursuing more advanced careers in my life. And I also thank so much my committee members, Dr. N.K. Anand and Dr. Y.A. Hasssan, for their supporting and encouraging me. I will not forget their kind and cheering words toward me.

The experimental set-up was built by Mr. H.S. Ahn and Mr. S.W. Lee. They always helped me whenever I needed their help for my thesis research from instrumentation to academic part. I am deeply grateful to them for their help.

I cannot help expressing my gratitude to my wife, Youchin. Thanks to her material and spiritual assistances, I could start and finish safely my graduate study in Texas A&M University. Especially, while muddling together through the bitters of life in Canada, we could build faith and love as firm as a rock through her endurance and courage. Love and faith were strong supports during my study.

I would like to say thank you to my lovely son, Youchan. He has been always pride and consolation for me and my wife. Even though he was young, my son always understood my situation and yield for my study.

I sincerely thank my dear friends, Keunmin and Kyuyong. During the stay in the U.S. for my study, they took care of my aged parents. Without their assistance, I could not study in peace and quiet without worries.

Most of all, I am much indebted to my father-in-law, mother-in-law, and brother-in-law. They sacrificed themselves to support me and my family for my study. They have always been my strongest supporter and comforter. The achievement of my graduate study and thesis was impossible without their generousities. I will never forget their love and devotion for me and my family.

## TABLE OF CONTENTS

	Page
ABSTRACT .....	iii
DEDICATION .....	iv
ACKNOWLEDGMENTS .....	v
TABLE OF CONTENTS.....	vi
LIST OF FIGURES .....	viii
LIST OF TABLES .....	ix
NOMENCLATURE.....	x
 CHAPTER	
I      INTRODUCTION .....	1
A. Background.....	1
B. Experimental Methodology.....	2
C. Review of Prior Research on Internal Cooling of Channel.....	4
1. Ribbed Wall.....	4
2. Channel with Pin-fins.....	6
3. Dimpled Wall.....	7
4. Channel with Blockages.....	8
D. Motivation of This Study.....	9
E. Outline of This Study.....	10
II     EXPERIMENTAL APPARATUS AND PROCEDURE.....	12
A. Experimental Apparatus .....	12
B. Experimental Procedure.....	19
C. Data Reduction.....	19
D. Uncertainty Analysis.....	21
III    EXPERIMENTAL RESULTS .....	22

CHAPTER	Page
A. Heat Transfer on Wall Segments.....	22
B. Friction Factors.....	27
C. Thermal Performance.....	29
IV RESULTS ANALYSIS.....	31
A. The Effect of Hole Area Ratio.....	31
B. The Effect of Hole Aspect Ratio.....	33
V SUMMARY AND CONCLUSIONS... ..	35
A. Summary.....	35
B. Conclusions.....	35
REFERENCES .....	38
APPENDIX A .....	42
APPENDIX B.....	45
VITA.....	55

## LIST OF FIGURES

FIGURE	Page
1	Schematic of test apparatus for heat transfer experiments (not to scale). .....12
2	Schematic of top and bottom walls of wide (12:1) rectangular channel with four blockages for this study. ....14
3	Blockages with elongated holes for Case S installed in test section to improve heat transfer rate: diameter of holes equals 3/4 of channel height .....15
4	Blockages with elongated holes for Case L installed in test section to improve heat transfer rate: diameter of holes equal 3/4 of channel height .....16
5	Average heat transfer enhancement on wall segments downstream of blockage .....23
6	Average value of average heat transfer enhancement on wall segments downstream of blockages .....25
7	Pressure drops across wall segments downstream of blockages relative to that for fully developed turbulent flow through a smooth channel without blockages .....28
8	Thermal performances of blockages with elongated holes – heat transfer enhancement per unit pumping power relative to that for fully developed flow through a smooth channel .....30
9	Pressure transducer calibration result .....54



## LIST OF TABLES

TABLE	Page
I	Dimensions of staggered hole arrays in the blockages in this study ..... 18
II	Hole area ratio effect - Nusselt number ratio increase rate ..... 32
III	Hole aspect ratio effect - Nusselt number ratio increase rate ..... 34
IV	Average Nusselt numbers obtained from heat transfer measurement ..... 42
V	Segmental friction factors obtained with heat transfer measurement ..... 43
VI	Thermal performances obtained with heat transfer measurement ..... 44
VII	Voltage and current readings of Type S for power consumption measurement 45
VIII	Voltage and current readings of Type L for power consumption measurement .. 46
IX	Voltage readings of Case S-1 for pressure drop measurement ..... 47
X	Voltage readings of Case S-2 for pressure drop measurement ..... 48
XI	Voltage readings of Case S-3 for pressure drop measurement ..... 49
XII	Voltage readings of Case L-1 for pressure drop measurement ..... 50
XIII	Voltage readings of Case L-2 for pressure drop measurement ..... 51
XIV	Voltage readings of Case L-3 for pressure drop measurement ..... 52
XV	Ambient, orifice, and inlet temperature measurement ..... 53
XVI	Voltage and current readings for segmented walls heat loss measurement ..... 53

## NOMENCLATURE

$a$	Width of elongated holes in blockages, $m$
$A_c$	Flow cross-sectional area of test channel, $m^2$
$A_s$	Surface area, $m^2$
$b$	Center-to-center spacing between adjacent holes in blockages, $m$
$d$	Diameter of holes
$D_h$	Hydraulic diameter of test channel, $m$
$f$	Friction factor
$f_0$	Reference friction factor for fully developed turbulent flow in smooth channel
$\bar{h}$	Average heat transfer coefficient, $W / m^2 \cdot K$
$H$	Height of test channel, $m$
$I$	Current, $A$
$k$	Thermal conductivity of air, $W / m \cdot K$
$\dot{m}$	Air mass flow rate, $kg/s$
$\overline{Nu}$	Average Nusselt number
$Nu_0$	Reference Nusselt number for fully developed turbulent flow in smooth channel
$\overline{Nu}_{average}$	Average Nusselt number of three segments at specific Reynolds number
$Pr$	Prandtl number
$q_{loss}$	Rate of extraneous heat losses, $W$
$Re$	Reynolds number
$\bar{T}_b$	Average bulk temperature, $K$
TP	Thermal performance

$TP_{average}$	Average Thermal performance of three segments at specific Reynolds number
$\bar{T}_w$	Average wall temperature, $K$
$V$	Voltage, $V$
$W$	Width of the test channel, $m$

### **Greek Symbols**

$\Delta p$	Pressure drop across two consecutive blockages, $N/m^2$
$\Delta x$	Distance between two pressure taps, $m$
$\rho$	Density of air, $Kg/m^3$

## CHAPTER I

### INTRODUCTION

#### A. Background

Gas turbine vanes and blades are exposed to high air temperature. And increasing turbine rotor inlet temperature directly leads to raise thermal efficiency and output power of gas turbines. The rotor inlet temperature is far higher than the melting point of the blade material. Hence, cooling technology of turbine blades has become one of the most important key factors for improvement of gas turbine engine efficiency since 1970s. To increase the gas turbine inlet temperature, two different prime directions have been pursued. The one is cooling technology as mentioned above and the other is to develop super-alloys or thermal barrier coating with higher thermal resistance. According to Takeishi [1], cooling technology enables turbine inlet temperature to increase by 25 °C per year but the achievement of super-alloy development technology limits by 10 °C per year. Thus to study cooling technology is more effective than to develop higher thermal resistance materials for gas turbine improvement.

Gas turbine blades are cooled by the air directly extracted from the engine compressor. This extracted air cause disadvantage of thermal performance by incurring pressure drop. Hence, Optimized cooling technique is needed considering operating conditions. Diverse cooling methods have been developed and can be grouped into two methods - internal and external cooling. Internal cooling can be performed by passing the extracted air from compressor through several serpentine passages inside blades and moving out the heat from blades. A number of internal cooling techniques have been developed. In the early period of gas turbine engines, only jet impingement cooling method was used for the leading edge cooling of blade. Jet impingement cooling is to cool blade by air impingement on the surfaces of serpentine passages. Impinging was most effective cooling method for leading edge making other methods unnecessary. But as gas turbine technology has been developed, the rotor inlet temperature has been also increased for turbine engine efficiency. Therefore, internal cooling technologies using

turbulators such as ribs and pin-fins have been developed. Due to highest thermal stress, leading edge cooling must be performed using jet impingement cooling but ribbed and pin-fined passages can be used for trailing edge cooling because holes for jet impinging was impossible due to structural problem of narrow passages comparing with the leading edge passages.

## B. Experimental Methodology

Actual turbine tests incur tremendous instrumentation and operational costs. Thus researchers have conducted simulated experiments similar to that in actual turbines and measured heat transfer coefficients or wall temperatures for low temperature experiments. Thus the data under the low temperature conditions can be scaled to real engine flow conditions by designers. The results are typically expressed in nondimensional parameters such as Nusselt number, heat transfer coefficient ratio, or temperature ratio.

From the design concept for gas turbine blades, most ideal situation is that gas turbine blade is run under the temperature as close to as the melting point of turbine blade alloy for reliable operation and at the same time the amount of coolant is as small as possible for gas turbine engine efficiency. For those purposes, blade designers must be able to obtain the local surface temperature distribution of the blades as well as the average level of temperature by performing heat transfer experiments and data analysis. Various experimental methods for measuring the wall temperature under the condition of steady or transient state have been contrived by a number of researchers. Among them, the representatives are: (1) diverse heaters with thermocouples, (2) optical surface visualization technique - liquid crystal thermography method, (3) naphthalene sublimation method.

Thermocouple techniques can provide direct temperature measurements on surface of heat transfer. Han and Park [2] conducted their experiments with the thin foil heater with thermocouples to measure local temperature distribution and calculate local heat transfer coefficients for the fully developed flow of rectangular channels with various rib turbulators. Han and Zhang [3] measured and calculated regional averaged temperatures, heat transfer coefficients and enhancement in a square channel with various rib turbulators for fully developed turbulent flow with copper plate heaters with thermocouples. VanFossen [4] researched the heat transfer enhancement effect of a

rectangular channel with several staggered short pin-fins arrays. He used electric heaters encased in a polyimide base film and thermocouples.

Optical measurement techniques are nonintrusive in which the test surface can be observed from outside from outside the flow path. Liquid crystal surface temperature measurement technique is one of the popular techniques for measuring local temperature distribution on channel wall under a steady or transient condition. Liquid crystals are thermo-chromic since they can express different colors selectively when the surface temperature under our consideration changes. At any particular temperature, liquid crystals reflect a single wavelength of light. The colors can be calibrated to specific temperatures since the transition of colors is sharp and precise. Taslim and Spring [5] used liquid crystal technique under the steady state to measure the effect of profile and spacing of transverse ribs for local heat transfer distribution in a channel. Kukreja and Lau [6] measured local temperature distribution and calculated local heat transfer coefficients for fully developed turbulent flow in internal ribbed passages of gas turbine blade using the transient liquid crystal method.

Mass transfer measurement technique uses the change of concentration of a fluid or solid medium. Hence, mass transfer can be understood as a phenomenon which occurs due to a concentration gradient between two regions. Momentum transport occurs at the interface of these two regions. This can be analogized to the momentum transport which occurs between the surfaces of a hot body and its surroundings by a temperature gradient which causes consequently the hot body to lose heat. The naphthalene sublimation technique has been used as the one of the mass transfer measurement techniques. One of advantages of this technique is to provide high resolution by eliminating heat loss and axial conduction effect since no heating of the surface or the fluid is required. Kukreja et al. [7] and Lau et al. [8] researched local heat-mass transfer distribution for a square channel with V-shaped ribs and for a rectangular channel with pin-fins respectively using naphthalene sublimation method. Lau et al [9] also measured heat transfer enhancement effect for turbulent flow in a rectangular channel in which blockages with staggered round and square holes were installed.

## C. Review of Prior Research on Internal Cooling of Channel

### 1. Ribbed Wall

Through the survey results provided by Han et al. [10] and Lau [11], heat transfer enhancement effect using diverse turbulators including ribs, pin-fins and impinging jets with or without rotation of channel has been studied by a number of researchers. Studies for heat transfer enhancement of internal channel flow installed with ribs with various configurations and parameters including channel aspect ratio, rib height to hydraulic diameter ratio, rib pitch to height ratio, rib height to width ratio, rib angle of attack, and blockage ratio.

Han and Park [2] studied the effect of rib angle of attack and channel aspect ratio for local heat transfer distribution in rectangular channels in which ribs were cast on the two opposite walls. For rib angles of attack,  $90^\circ$ ,  $60^\circ$ ,  $45^\circ$  and  $30^\circ$  were adopted and for channel aspect ratio, 1, 2 and 4 were chosen for their research. Their experiments were run under the condition of small channel length to hydraulic diameter ratios which range from 10 to 15. Result was that  $60^\circ$  angle of attack showed the highest average Nusselt number but also accompanied the highest pressure drop for the rectangular channel with aspect ratios 1 and 2, whereas for the transverse ribs, the highest Nusselt number was observed at an aspect ratio of 4. They postulated these different results came from the secondary flow induced by the angled ribs. As the channel aspect ratio increased the secondary flows induced by the ribs with angle of attack on the opposite walls were cancelled out each other due to the reduced channel height, whereas for the aspect ratio 1 and 2 of the rectangular channel, the secondary flows could enhance the heat transfer from walls. They could also provide that the ribs with an angle of attack  $30^\circ$  for the square channels and  $45^\circ$  for the rectangular channels with aspect ratios of 2 and 4 results in highest heat transfer per unit pumping power respectively.

Lau et al. [12] studied collectively the heat transfer enhancement, friction factor and thermal performance of square channels walls for fully developed turbulent flow with various angles of attack of high performance V-shaped ribs placed on two opposite walls. Angle of attack of  $45^\circ$ ,  $60^\circ$ ,  $90^\circ$ ,  $120^\circ$  and  $135^\circ$  were examined for their study and for the rib pitch to height ratios, 10 and 20 were used for parallel or crossed rib arrays on the two opposite walls. Conclusion was that the  $60^\circ$  V-shaped ribs with a rib pitch to height ratio of 10 showed the highest heat transfer and thermal performance even though

it caused a higher pressure drop than the corresponding angled full ribs and transverse full ribs, whereas the reverse V-shaped ribs for which rib angles of attack was more than  $90^\circ$  induced high pressure drop and thus low thermal performances. They could postulate that the ribs crossing on the two opposite walls enhanced neither heat transfer nor thermal performance. And increasing the rib pitch to height ratio decreased the ribbed wall and also smoothed wall heat transfer, friction factor and thermal performance.

Kukreja and Lau [7] measured local heat transfer for turbulent flow in a straight square channel with solid and perforated ribs on two opposite walls. They conducted experiments using  $60^\circ$  and  $90^\circ$  solid and perforated ribs and  $60^\circ$  solid V-shaped ribs for a height to hydraulic diameter ratio of 0.125 of the channel and a rib pitch to height ratio of 10. They concluded that the perforated ribs could not enhance heat transfer comparing with the solid ribs since the jet flow passing through the holes reduced the strength of flow reattachment on the wall downstream of a rib. Consequently although the lower pressure drop caused by the perforated ribs, substituting the solid ribs with the perforated ribs did not improve thermal performance due to the weakened reattachment flow. The result also showed that increased hole size, the number of holes and total hole area did not affect the overall heat transfer enhancement. V-shaped ribs were recommended for gas turbine internal cooling solution by them.

Buchlin [13] provided the effect of various configuration of the perforation, pitch of the perforated ribs, and the ratio of the clearance area to the total frontal area of the ribs for heat transfer on a wall of a wind tunnel by conducting experiments with five different shapes of perforated ribs. An enhancement of local heat transfer downstream of the perforated ribs could be observed comparing with the corresponding the solid ribs. Hence, the author could recommend a chevron type perforation as an optimal perforated holes design for perforated ribs.

A critical design point for turbine airfoil is the restriction in size and shape of the leading and trailing edges under the consideration of aerodynamics of the airfoils. Hence, the design of turbulator blockage is subjected to the airfoil design. The turbulator blockage ratio which is same as height to channel hydraulic diameter ratio is usually greater than 0.2. Bailey and Bunker [14] measured heat transfer and friction factor of the channel walls by studying the effect of the turbulator blockage ratios which ranged from 0.193 to 0.333. They conducted their experiments using  $45^\circ$  staggered turbulators in a rectangular channel of an aspect ratio of 0.4. During their experiments they kept turbulator pitch to height ratio constant of 10 for all rib configurations. The result was



that the turbulators with a high blockage ratio enhanced Nusselt number up to 3.6 comparing with that of a smooth channel, whereas the turbulators also caused higher friction factor reaching to 65. The channel with 45° high blockage ratio turbulators on the two opposite walls had lower Nusselt number than that of the 90° transverse turbulators at the same blockage ratio.

## 2. Channel with Pin-fins

Considering the design limitation of turbine blade and based on the cooling techniques, there are three major internal cooling zones in a turbine blade. The leading edge is cooled by jet impingement, the middle portion is cooled by serpentine ribbed channel and the trailing edge is cooled by pin fins. The basic concept for using pin fins is to increase internal wetted surface area and to enhance turbulence intensity. The heat transfer process by pin fin is that pin fin increases heat transfer by transmitting the heat from the walls to the flowing air passing through between the consecutive pin fins aligned in each row. The main parameters for pin fin cooling technique are pin height to diameter ratio, streamwise pin spacing to diameter ratio and spanwise pin spacing to diameter ratio.

Armstrong and Winstanley [15] conducted experiments for heat transfer and friction factor of a channel wall installed with a staggered array pin fin. The authors provided the effect of pin height to diameter ratio and pin spacing as geometric parameters affecting heat transfer and friction factor. After review of the prior studies of VanFossen [4], Metzger and his associates [16,17,18,19], and Zukauskus [20], they concluded that the average heat transfer over pin fins array correlates with Reynolds number to a power of 0.6 and 0.7 depending on pin height to diameter ratio. The research of Brigham and VanFossen [21] verified the result that heat transfer was not affected by the pin height to diameter ratio for the ratio less than two, whereas the pin height to diameter ratio for a ratio greater than two can increase heat transfer. Based on their experiments they could speculate that the heat transfer for short pin fins was dominated by the endwall interaction and that for long pin fins was dominated by the cylinder interaction respectively. For friction factor, they recommended Metzger's correlation [18] for a large range of pin height to diameter ratios and pin spacings.

In the middle of turbine blade trailing edge cooling, some of the coolant is ejected from the channel through small holes along trailing edge and the rest is ejected through

the blade tip. Lau et al. [22, 23] conducted experiments for measuring heat transfer and pressure drop in a pin fin channel with ejection holes. Heat transfer and pressure drop results for a number of channels with various ejection holes and slot geometries were produced. Lau et al. [24] showed the result of heat transfer and friction factor affected by lateral flow ejection for fully developed turbulent flow in pin fin channels. They examined regional heat transfer for ejection holes with several sizes and numbers through the side wall of the test section which consisted of a rectangular channel having staggered arrays of eight streamwise rows of pins. They used a pin height to diameter ratio of 1 and a spanwise pin spacing of 2.5 forming an equilateral triangles array. Based on their experimental results, they could postulate that when coolant came out from the ejection holes, the regional heat transfer dropped much faster along the segments in a streamwise direction than the case without ejection holes. They thought this is due to the decrease in the mass flow rate ejected from channel outlet. They also showed that increase of the size or number of the ejection holes causes drop of overall heat transfer and friction factor of the channel.

### 3. Dimpled Wall

As one of innovative techniques for turbine blade internal cooling, dimpled surface with diverse design parameters such as the ratio of channel height to dimple print diameter and the ratio of dimple depth to dimple print diameter has been studied. Most remarkable advantage of this method is to enhance heat transfer with relatively small pressure drop penalties by not blocking main stream of coolant comparing with other turbulators.

Ligrani and Mahmood [25] provided spatially resolved distributions of local Nusselt numbers, instantaneous flow structure from flow visualization, and distributions of total pressure and streamwise velocity for locations along the dimpled surface at different Reynolds number, and at different ratios of air inlet stagnation temperature to local surface temperature. In this study flow visualizations showed vortical fluid and vortex pairs shed from the dimples, including a large upwash region and packets of fluid emanating from the central regions of each dimple, as well as vortex pairs and vortical fluid from than form near dimple diagonals. These vortex structures augmented local Nusselt numbers near the downstream rims of each dimple, both slightly within each depression, and especially on the flat surface just downstream of each dimple.

Mahmood [26] also investigated the local heat transfer enhancement of dimpled surface with ratios of channel height to dimple print diameter of 0.20, 0.25, 0.50, and 1.00 for fixed the ratio of dimple depth to dimple print diameter, 0.2. The result showed vortex pairs periodically shed from the dimples were stronger as non dimensional channel height  $H/D$  decrease for given Reynolds numbers about 600 to about 11,000. This also led to local Nusselt number augmentations at these same locations.

The effect of the ratio of dimple depth to dimple print diameter was estimated by Ligrani and Burgess [27]. They studied dimpled test surfaces placed on the wall of different rectangular channel. The test were conducted to provide information on influences of dimple depth using the ratios of dimple depth to dimple print diameter of 0.1, 0.2, and 0.3 for fixed the ratio of channel height to dimple print diameter, 1.0. The results showed local heat transfer enhancement occurred as the dimple depth increase at all Reynolds number considered (9,940 to 74,800).

#### 4. Channel with Blockages

Blockages with various holes as a one of diverse turbulators have been developed. The coolant passing through a channel hit the surface of the walls of blockages. This process can be understood as an impinging phenomenon leading to enhancement of heat transfer and pressure drop. Although the blockages with holes incur the pressure drop depending on the holes configuration, overall thermal performance can be increased by enhancement of convective heat transfer from the walls caused by combination of impinging effect and flow mixing.

Moon and Lau [28] provided local heat transfer distribution for a rectangular channel installed blockages with holes to make turbulent flow using a liquid crystal method. Nine different staggered arrays of holes were placed on blockage wall surfaces and experiments were conducted to measure the effect of holes configurations. The results showed that the blockages enhanced heat transfer by 5 to 8 times comparing with a smooth channel without blockages, whereas significant pressure drop across the blockages was induced. Due to the pressure drop, the heat transfer of a channel with blockages per unit pumping power was lower than that without blockages. The result also showed that the local heat transfer distribution was strongly dependent on the hole configuration in the blockages of a channel.

Lau et al. [9] performed experiments for heat transfer enhancement of a channel

wall by blockages with staggered round and square holes for turbulent flow in a rectangular channel using mass transfer method. They used the naphthalene sublimation method to measure averaged and local heat (mass) transfer on the wall. The result showed that convective heat transfer enhancement reached to 5 to 6 times for a fully developed turbulent flow comparing with a smooth channel, whereas pressure drop was increased significantly up to 490 times for a smooth channel. Also heat transfer enhancement was higher in the blockages with square holes than with round holes.

#### D. Motivation of This Study

There has been no study on convective heat transfer for turbulent air flow through blockages with holes in a channel of gas turbine blade except for Moon and Lau [25] and Lau et al. [9]. However Moon and Lau [25] conducted their experiments to see the effect of blockages with round holes depending on holes size and round holes configurations and measured local heat transfer distribution on the wall of a rectangular channel and pressure drop across two consecutive blockages. In a similar way, but using a different wall temperature measurement method, Lau et al. [9] examined heat transfer enhancement on a channel wall installed with blockages with round and square holes. Hence it is interesting to study the effect of hole aspect ratio (the ratio of width to height of hole) and area ratio (the ratio of the hole area to whole surface area of a blockage) affecting heat transfer enhancement and pressure drop across two consecutive blockages with holes.

Hence, the purpose of this study is to measure average heat transfer enhancement, pressure drop across two consecutive blockages and thermal performance on the three principal walls between blockages for fully developed turbulent flow in a rectangular channel by investigating the effects of the aspect ratio of the holes in blockages and area ratio. These four blockages were installed perpendicular to the direction of the main coolant flow in a wide rectangular channel. Thus blockages had the same cross section as the rectangular channel. Copper plate heaters with seven embedded thermocouples respectively were used to measure averaged heat transfer of the channel wall at Reynolds numbers of 7,000, 12,000 and 17,000. Pressure drops across two consecutive blockages were also measured to calculate the thermal performance of the blockages.

## E. Outline of This Study

As a new method for turbine blade internal cooling, blockages with staggered elongated holes were brought into a rectangular channel with an aspect ratio of 12 and installed perpendicularly to the main flow direction to measure their effect on average heat transfer, friction factor, and thermal performance for fully developed turbulent flow at Reynolds numbers of 7,000, 12,000, and 17,000. For this study, aspect ratios of 1.55, 1.99, and 2.88 were used for the blockages with the area ratio of 0.5 and 1.81, 2.35, and 3.41 for the blockages with the area ratio 0.6 as main parameters. Aspect ratios were decided by the number of holes of a blockage. For each area ratio of a blockage surface, three different cases of blockages having four holes, six holes, and eight holes were designed. Hence, total six sets of experiments were conducted. All holes shapes were elongated types and round type holes were eliminated since the purpose of this study was to investigate the effect of blockages with holes incurring the least pressure drops. As mentioned previous section, blockages with round hole caused higher pressure drop than those with elongated holes. Experiments were performed using three copper plate heaters embedded twenty one thermocouples to investigate averaged segmental heat transfer enhancement, three regional averaged pressure drops between two consecutive blockages and consequently three regional thermal performances. Pressure drops across two consecutive blockages were measured with a pressure transducer. Those pressure drops were used to calculate heat transfer per unit pumping power, i.e., thermal performance. The summary of performed experiments to measure and calculate heat transfer enhancement, pressure drops (friction factor ratios) and heat transfer per unit pumping power (thermal performance) of a rectangular channel wall for fully developed turbulent flow is as follows:

1. To measure averaged regional heat transfer on the rectangular channel wall, experiments using copper plate heaters with twenty one embedded thermocouples were conducted. Only elongated hole type blockages were used for these experiments. Three different numbers of holes, i.e., four, six, and eight holes deciding three different cases, i.e., hole-width-to-height aspect ratios, were adopted for each type of blockages having area ratios of 0.5 and 0.6 respectively. Hence, total six sets of blockages were used for these experiments.

2. Pressure drops across two consecutive blockages with six different configurations of holes were measured using a pressure transducer.
3. Thermal performances for the three segmental sections of a rectangular channel were calculated using Nusselt number and friction factor ratios.

## CHAPTER II

### EXPERIMENTAL APPARATUS AND PROCEDURE

#### A. Experimental Apparatus

The main elements of this test apparatus for this experiment were the test section, a chamber for flow settlement, an orifice flow meter, a control valve, and two centrifugal blowers as shown in Figure 1. The test section was an wooden rectangular channel having a cross section of  $30.5\text{ cm}$  width by  $2.54\text{ cm}$  height referred to as having an aspect ratio of 12:1. The walls of a rectangular channel were constructed of  $1.27\text{ cm}$  thick oak plywood.

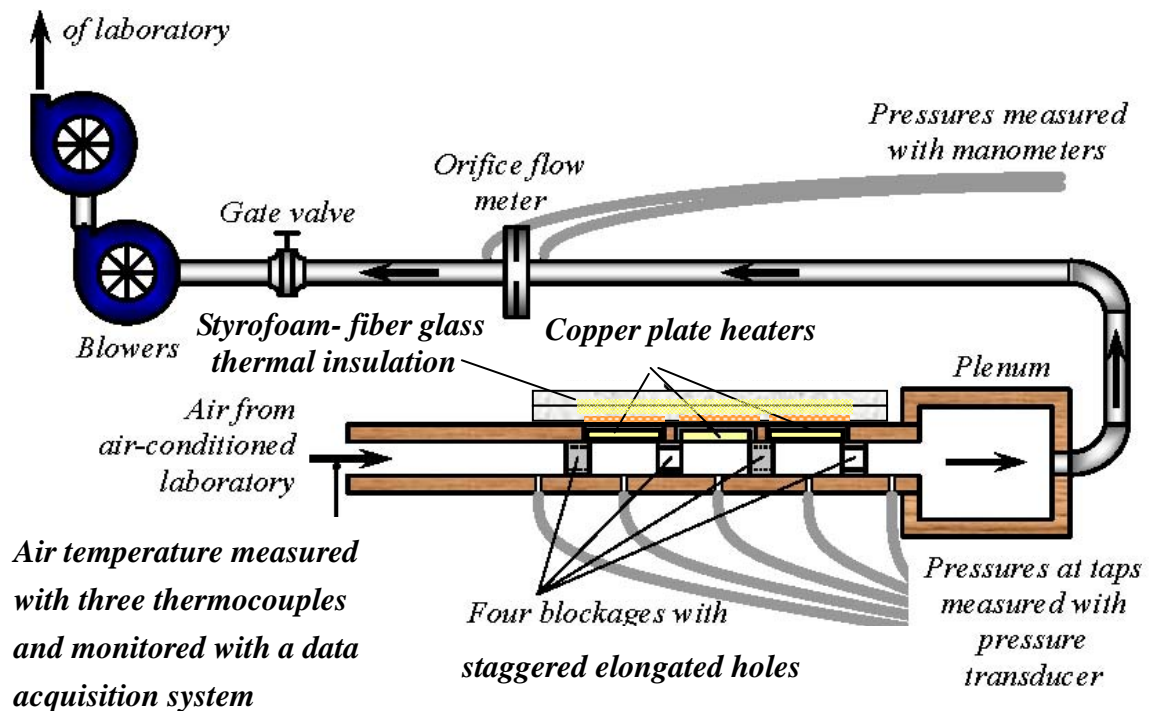


Fig. 1. Schematic of test apparatus for heat transfer experiments (not to scale).

As shown in Figure 2(a), three removable copper plates insulated in Balsa wood were installed into the prepared slots and composed the top wall of the rectangular channel. Each copper plate measured  $5.08\text{cm}$  by  $30.5\text{cm}$  and was  $1.27\text{cm}$  in thickness. During the experiments, copper plates were heated by flexible electric heater attached on the top of the each plate with silicon rubber adhesive. Balsa wood was used as thermal insulation to protect conduction between copper plates. This wood measured thickness of  $3.2\text{cm}$  and was attached onto the four edges of each copper plate also with silicon rubber adhesive. The gap on the top of the plates between copper plates and Balsa wood were sealed using silicon sealant to reduce heat loss to environment.

After the copper plates were installed into the three slots of the top wall of the test section, the top of the three copper plates array were covered with fiberglass. To eliminate possible minute gap and air leakage between Balsa wood enclosing copper plates and blockages, clamps were used since this kind of gap can induce hydraulic and thermal boundary on the copper plate surfaces. Over the fiberglass, Styrofoam insulation cover fit for the top of the test section to minimize heat loss to surroundings was used.

As shown in the schematic of the top view of the test section removed top wall in Figure 2(b), four blockages with elongated holes were installed in the rectangular channel with the same spaces of  $5.08\text{cm}$ . These blockages had the same cross section as the cross section of the rectangular channel. The blockages were made of acrylic and had  $1.14\text{cm}$  thickness, and the distance between two consecutive blockages was equal to  $5.08\text{cm}$  as mentioned above. The figure of  $5.08\text{cm}$  was equal to the two times of the height of the rectangular channel. To make secondary flow when the coolant passes through the holes of blockages, the elongated holes of the blockages were arrayed staggeringly also as shown in Figure 2(b). These secondary flows played the role of enhancing heat transfer from the copper plate walls.

For the measurement of averaged pressure difference between internal pressure of the rectangular channel and atmosphere pressure, fifteen pressure taps were installed on the bottom of test section as shown in Figure 2(b). Three pressure taps were located respectively on the three segmental sections between two consecutive blockages with appropriate distances.

The first blockage was placed at  $26.0\text{cm}$  from the entrance of the rectangular channel. The holes of the blockages were to be arrayed in staggered way inside the channel by alternately installing the two different kinds of blockages in the same case as shown in Figures 3 and 4. The impinging effect and increased coolant mixing rate were



caused by the staggered holes arrays.

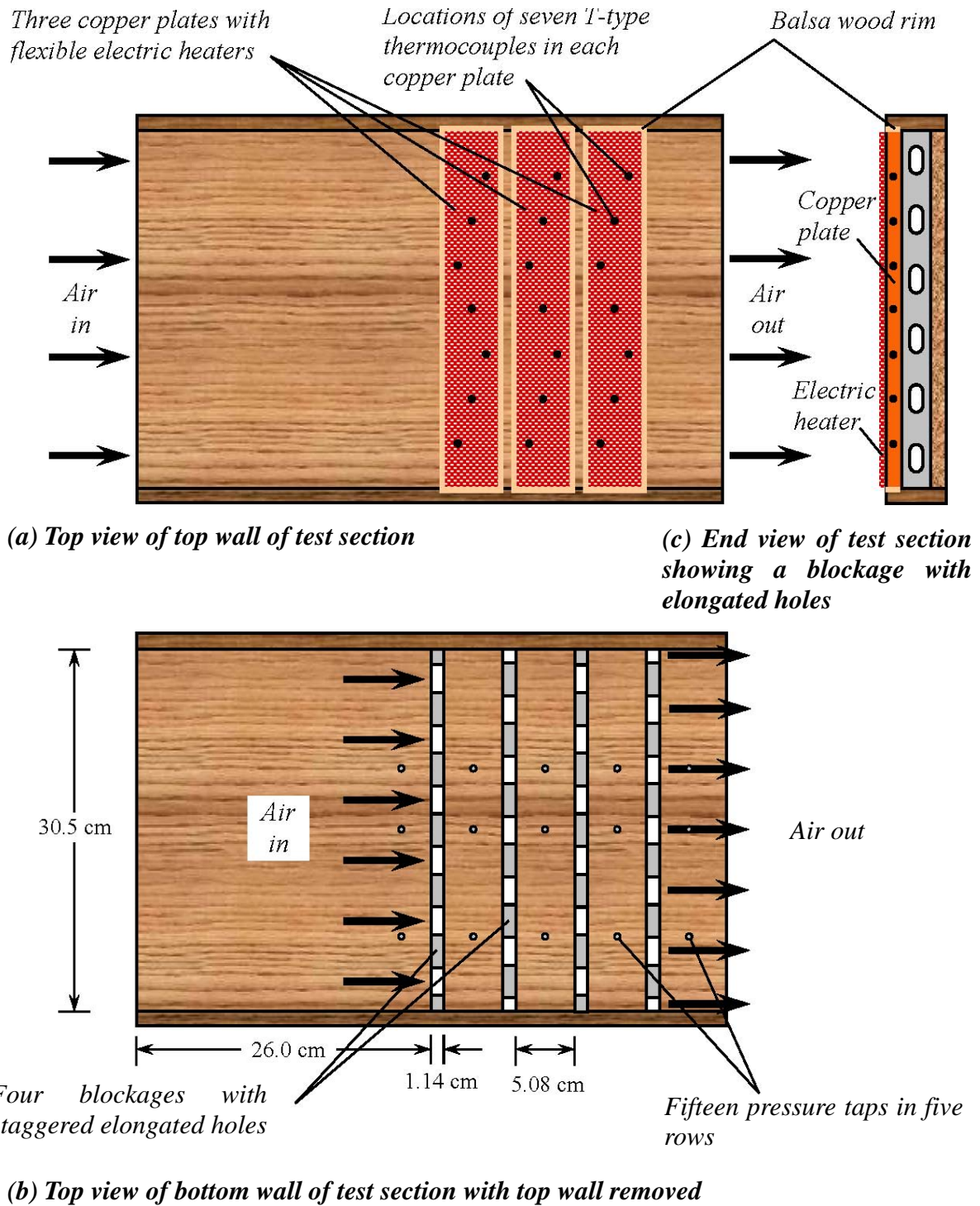
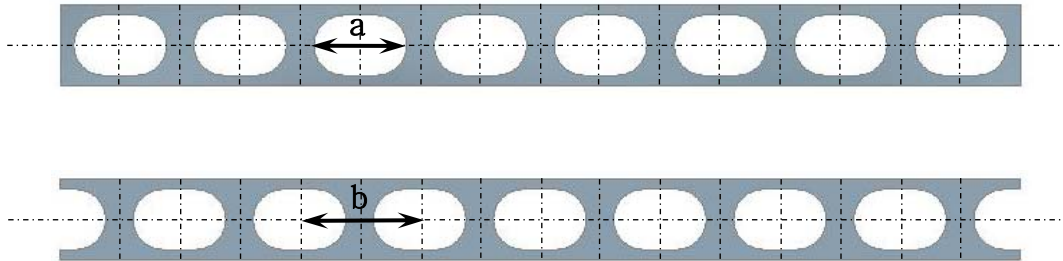
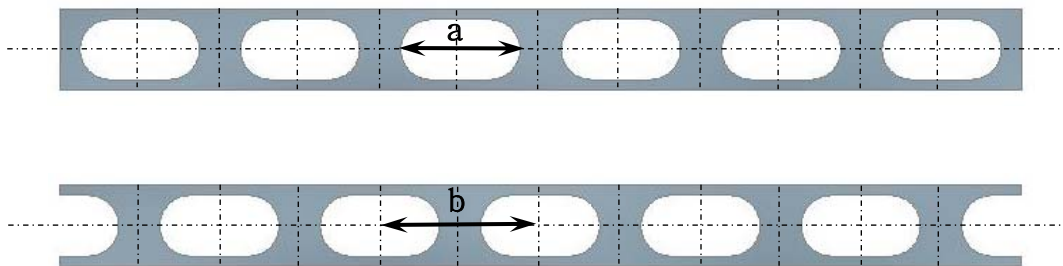


Fig. 2. Schematic of top and bottom walls of wide (12:1) rectangular channel with four blockages for this study.

*Blockages with eight 2.95 cm × 1.91 cm elongated holes*



*Blockages with six 3.78 cm × 1.91 cm elongated holes*



*Blockages with four 5.49 cm × 1.91 cm elongated holes*

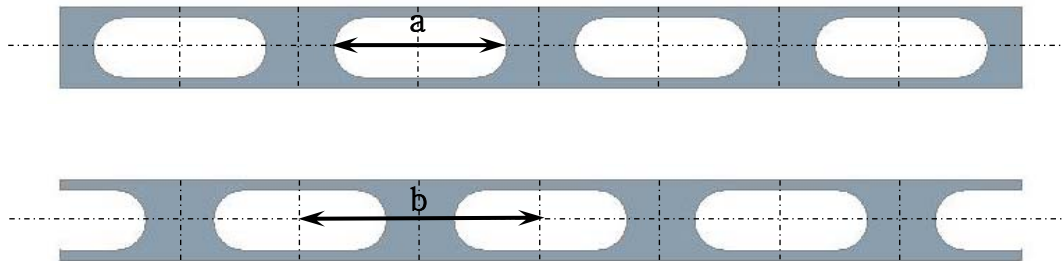


Fig. 3. Blockages with elongated holes for Case S installed in test section to improve heat transfer rate: diameter of holes equals 3/4 of channel height.

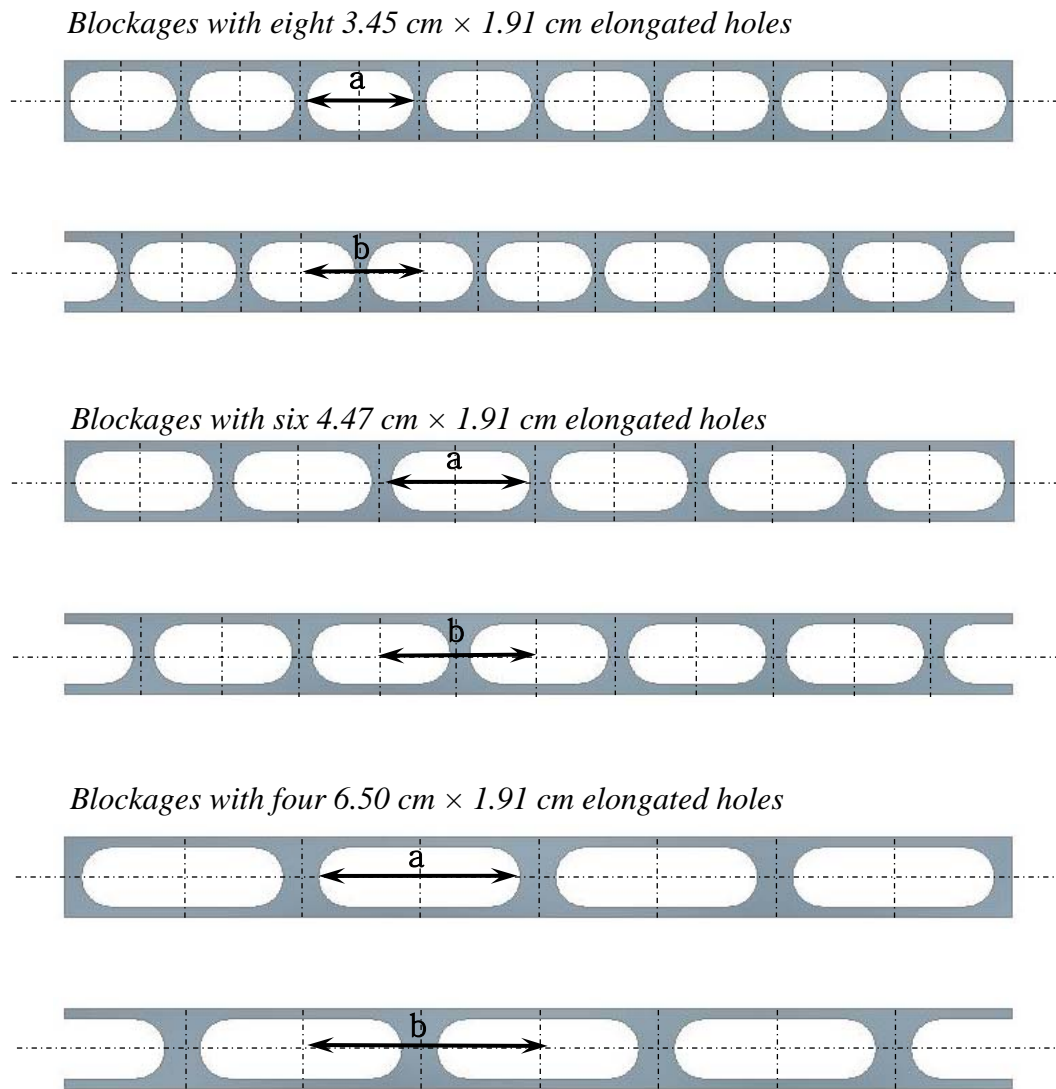


Fig. 4. Blockages with elongated holes for Case L installed in test section to improve heat transfer rate: diameter of holes equals 3/4 of channel height.

For the six sets of blockages with respective different hole configurations, experiments were conducted. But for this research, the elongated holes of the four blockages had all the same diameter of  $1.91\text{ cm}$ , or  $3/4$  of the channel height. The dimensions of the elongated holes and the distances between the holes are listed in Table 1. The area ratio, the ratio of total cross-sectional hole area to whole cross-sectional blockage surface area per a blockage, were kept constants of 0.5 or 0.6 while the aspect ratios increased respectively in three steps. Thus as aspect ratios increased in three stages, also the total number of holes inversely decreased by two holes from eight up to four.

In this study, two different types, i.e., shorter hole type (Case S) and longer hole type (Case L), which were classified based on the two different hole-to-blockage area ratios of 0.5 and 0.6 defined as the ratio of total hole cross sectional area to blockage surface area perpendicular to flow direction of the main stream, were considered. The reason why the two different types were named as shorter and longer hole types was that the number of holes and the center of holes were same each other between corresponding cases, i.e., Case S-1 and L-1, Case S-2 and L-2, and Case S-3 and L-3 respectively. The only different aspect between corresponding cases of the two different hole-to-blockage area ratios was the width of hole. Thus the hole-to-blockage area ratio of 0.5 was named as Case S (shorter hole type) and that of 0.6 as Case L (longer hole type). And in accordance with the hole aspect ratio which can be defined as hole width to height ratio, each types were subdivided into three different cases respectively ,i.e., Case S-1(four holes), S-2(six holes), and S-3(eight holes) for Case S and Case L-1(four holes), L-2(six holes), and L-3(eight holes) for Case L. Total six different hole aspect ratios were considered for this study as shown in Table I.

Air was used as the working fluid. During the experiments, air was drawn through the test section by the two centrifugal blowers which were connected each other in series and exited the test apparatus to the outside of the building in which the laboratory is located. The two centrifugal blowers were located inside of air ventilation facility to reduce the affect of increasing the inlet temperature by heated air from the blowers.

Three thermocouples were located at the entrance of the rectangular channel with the same distances to measure inlet temperatures. One thermocouple for ambient temperature was installed in the flow free region. Another thermocouple was installed in orifice flow meter to calculate mass flow rate. Hence, total twenty six thermocouples were monitored with computer controlled data acquisition system throughout the duration of the experiments. Before experiments, all thermocouples were calibrated with

a constant thermal bath against a calibrated standard which was traceable to NIST.

Table I. Dimensions of staggered hole arrays in the blockages in this study

Shorter holes, $d=1.91\text{cm}$	Case S-1	Case S-2	Case S-3
Number of holes	8	6	4
Width of holes, "a"(cm)	2.95	3.78	5.49
Center to Center spacing, "b"(cm)	3.81	5.08	7.63
Cross-sectional Area( $\text{cm}^2$ )	4.83	6.43	9.67
Hole-to-blockage area ratio	0.5	0.5	0.5
Hole aspect ratio	1.55	1.99	2.88
Longer holes, $d=1.91\text{cm}$	Case L-1	Case L-2	Case L-3
Number of holes	8	6	4
Width of holes, "a"(cm)	3.45	4.47	6.5
Center to Center spacing, "b"(cm)	3.81	5.08	7.63
Cross-sectional Area( $\text{cm}^2$ )	5.80	7.74	11.61
Hole-to-blockage area ratio	0.6	0.6	0.6
Hole aspect ratio	1.81	2.35	3.41

## B. Experimental Procedure

For each experiment, using two TRMS digital multimeters, the voltage drops and currents of the copper plate heaters were measured and recorded after the temperature of copper plates went into the steady state (50°C). The temperatures of the number of twenty seven 36-gage T-type thermocouples embedded in the three copper plates were measured using a computer-controlled data acquisition system. The pressure drops across the blockages were measured through fifteen static pressure taps at five streamwise stations using a calibrated pressure transducer. Figure 2(a) also indicates the locations of the twenty-one thermocouples embedded in the three copper plates and the locations of the fifteen static pressure taps at five streamwise stations in the bottom wall of the channel.

Experiments were conducted to examine the average heat transfer coefficient on the wall segments of the channel downstream of the blockages and the pressure drops across the blockages for three different mass flow rates which were corresponded to Reynolds numbers of 7,000, 12,000 and 17,000. Experiments for calibrating the instruments for measuring the air mass flow rate, the wall and air temperatures, and pressures were performed separately. Preliminary test were conducted also to calculate heat loss under the steady state without air flow.

## C. Data Reduction

The average Nusselt numbers for each of the three wall segments of the channel between two blockages was calculated as

$$\overline{Nu} = \frac{\overline{h}D_h}{k} \quad (\text{C.1})$$

Where the averaged heat transfer coefficients were defined as

$$\overline{h} = \frac{IV - q_{loss}}{A_s (\overline{T}_w - \overline{T}_b)} \quad (\text{C.2})$$

The average Nusselt numbers were normalized using reference Nusselt number for

fully developed turbulent flow in the channel with smooth walls.

This reference Nusselt number was defined as:

$$Nu_0 = 0.023 Re^{0.8} Pr^{0.4} \quad (C.3)$$

Using the pressure gradients across the blockages, the friction factors were calculated as:

$$f = \frac{(\Delta p / \Delta x) D_h}{\rho \bar{u}^2 / 2} = 2 \rho \left( \frac{\Delta p}{\Delta x} \right) D_h \left( \frac{A_c}{\dot{m}} \right)^2 \quad (C.4)$$

Where  $\Delta x$  is the distance between two pressure taps across two consecutive blockages in [m],  $u$  is the average air velocity in [m/s], and  $A_c$  is the cross section area of the test channel in [m]. In this study, these friction factors were also compared with a reference friction factor for fully developed turbulent flow in the channel with smooth walls.

The reference friction factor was defined as:

$$f_0 = [0.79 \ln(Re) - 1.64]^{-2} \quad (C.5)$$

Using average Nusselt number and friction factor, thermal performance was defined as:

$$TP = (\overline{Nu} / Nu_0) (f / f_0)^{-1/3} \quad (C.6)$$

Thermal performance indicates the heat transfer enhancement by the blockages per unit pumping power comparing with the heat transfer for fully developed turbulent flow in the channel with smooth walls.

#### D. Uncertainty Analysis

Using the uncertainty analysis method from [29], the uncertainties of Reynolds number, Nusselt number, and friction factor were calculated with a confidential level of 95%. The uncertainty of air mass flow rate was estimated based on the uncertainties of  $\pm 1.0\%$  for all properties of air and  $\pm 0.5\%$  for all physical dimensions. The result of uncertainty for air mass flow rate was  $\pm 2.2\%$ . The uncertainties for Reynolds number, the heater voltage and current were calculated  $\pm 2.5\%$ ,  $\pm 2.2\%$ , and  $\pm 1.2\%$  respectively. For the average wall and bulk temperatures, the uncertainties were  $\pm 2.5\%$  and  $\pm 2.6\%$  respectively. Based on these uncertainties, the uncertainty for Nusselt number was  $\pm 6.0\%$ . For the maximum uncertainty of  $\pm 6.6\%$  for  $\Delta p$  and  $\pm 2.2$  for  $\dot{m}$ , the maximum value of the uncertainty for the friction factor was  $\pm 8.3\%$ .



## CHAPTER III

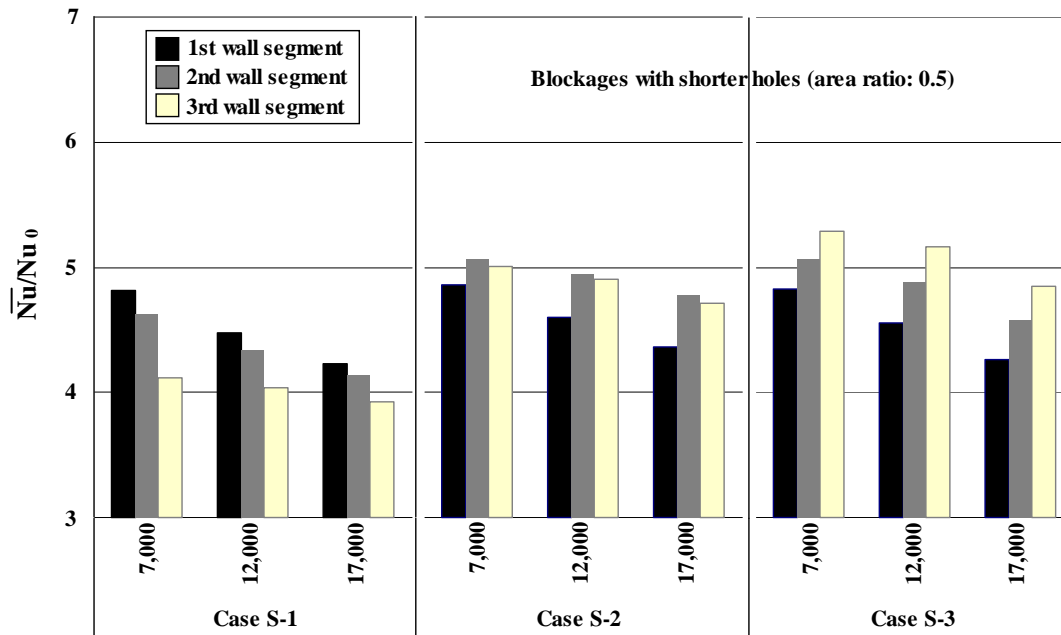
### EXPERIMENTAL RESULTS

#### A. Heat Transfer on Wall Segments

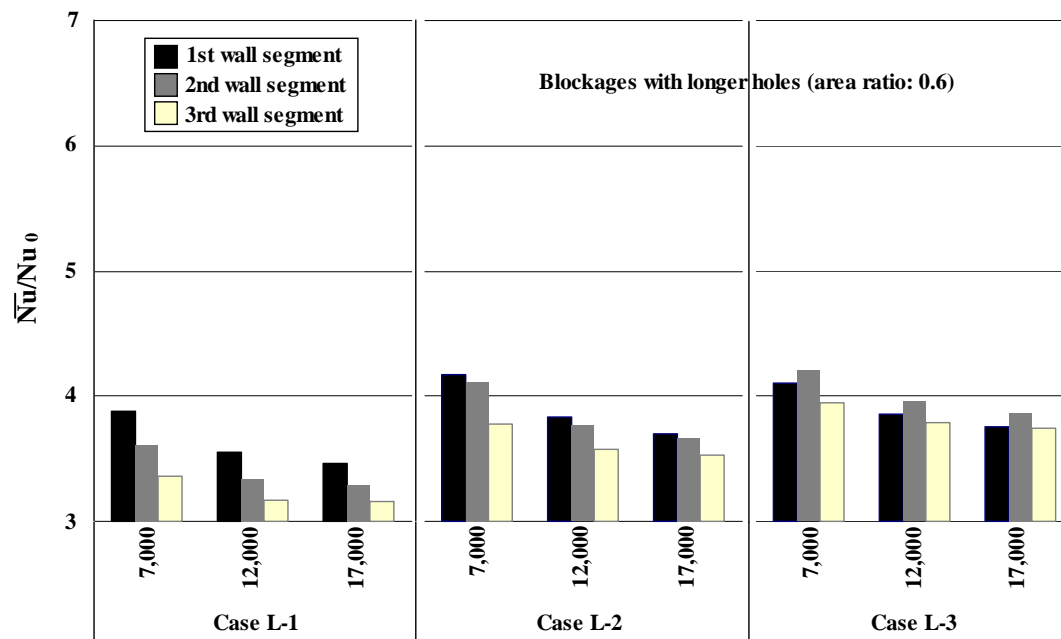
In this study, average convective heat transfer coefficients for the three wall segments composed of three copper plates with total twenty one embedded thermocouples were determined. These segments were divided by four staggeringly arrayed blockages. Six different cases of blockages, i.e., three hole width-to-height aspect ratios of blockages per one of the two hole-to-blockage area ratios, were tested. Based on the power of two centrifugal blowers connected in series, this study was performed for three different air flow rates, i.e., three different Reynolds numbers. Pressure drops were also measured by using fifteen pressure taps connected to pressure transducer. The effect of average convective heat transfer enhancement by blockages was expressed by Nusselt number ratio. The results of pressure drops were shown with friction factor ratios. These two parameters, Nusselt number and friction factor ratios, were also used to calculate thermal performance, TP.

Figure 5 shows average Nusselt number ratios on each segmented walls sectioned by blockages with six different hole configurations. The  $\overline{Nu}/Nu_0$  values at the three different Reynolds numbers of about 7,000, 12,000, and 17,000 are provided for the six different cases of blockages – (a) Cases S-1 through S-3 for the blockages with the smaller area ratio, 0.5 and (b) Cases L-1 through L-3 for the blockages with the larger area ratio, 0.6. In all cases, as Reynolds number increases, Nusselt number ratio ( $\overline{Nu}/Nu_0$ ) on each segmented wall decreases. In other words, as the air flow rate increases, the heat transfer enhancement decreases. These results also confirm that even though average convective heat transfer coefficient for forced convection increases proportionally to Reynolds number, the increase rate of reference Nusselt number ( $Nu_0$ ) surpasses it.

The average Nusselt number ratios were not always higher on the first wall segment between the first two blockages than on the other two downstream wall segments. In the cases of area ratio 0.5, the average Nusselt number ratio on the



(a)



(b)

Fig. 5. Average heat transfer enhancement on wall segments downstream of blockages.

first segment is the highest only for the blockages with four holes, whereas in cases of area ratio 0.6, the average Nusselt number ratio on the first wall segment is highest for blockages with four or six holes. Heat transfer enhancement, the average Nusselt number ratios of the blockages with four or six holes in case of the area ratio 0.5 on the second and the third wall segments, were superior to the first segment. The trend of graph among the cases of area ratio 0.5 means that impinging and turbulent mixing effect of blockages is gradually developed downstream of the blockages as the aspect ratio increases. And the turbulent effects on the second and the third wall segments were similar to those with the blockages of aspect ratio 1.99 and area ratio 0.5. At the aspect ratio of 2.88 of area ratio 0.5, the ranks of Nusselt number ratios on each segmented walls were inversely determined by the order of segments. With an increase of the aspect ratio of the holes, the corresponding Nusselt number ratios also significantly increase on the third wall segment. They remain about constant on the first wall segment within the difference of 2.4%, increase from 9.6% to 15.7% on the second wall segment as the aspect ratio increases from 1.55 to 1.99 (Case S-1 and S-2) but decrease as the aspect ratio increases 1.99 to 2.88 (Case S-2 and S-3).

Same explanation can be applied to the blockages with area ratio 0.6. Thus, for the blockages at the aspect ratio 3.41 (Case L-2) with the area ratio 0.6, mixing and impinging effect gets gradually enhanced downstream of the blockages. But for the blockages of area ratio 0.6, heat transfer enhancement effects on the first and the second wall segments were higher than that of the third wall segment for all cases in this study. As the aspect ratio increases, the corresponding values of Nusselt number ratios on the third wall segments increase like the cases with area ratio 0.5. But the increase rates of Nusselt number ratios on the first and second walls slow down. The values of Nusselt number ratios on three segmented walls divided by the blockages of aspect ratio 3.41 and area ratio 0.6 (Case L-3) were very close to each other at the same Reynolds number. The biggest difference of Nusselt number ratios among the segmented walls was just 6.2% between the second and the third segmented walls at Reynolds number 7,000. Figure 5 can be clearly interpreted as the variation of the averaged heat transfer coefficients on the three wall segments for the six different configurations of the holes in the blockages.

In figure 6, the  $\overline{Nu}_{average} / Nu_0$  values at the three different Reynolds numbers of about 7,000, 12,000, and 17,000 are provided for the six different cases of blockages –

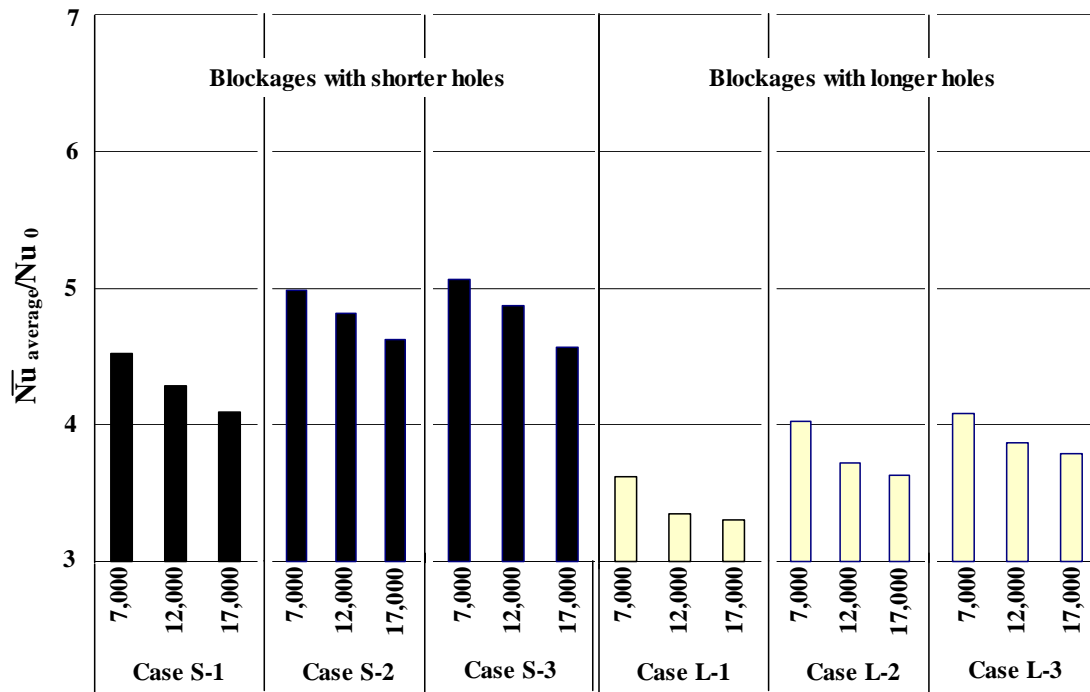


Fig. 6. Average value of average heat transfer enhancement on wall segments downstream of blockages.

from Cases S-1 to S-3 of the smaller area ratio, 0.5 and from Cases L-1 to L-3 of the larger area ratio, 0.6. When Reynolds number increases from about 7,000 to 17,000, the average value of average Nusselt number ratios ( $\overline{Nu}_{average} / Nu_0$ ) on the three segmented walls decrease by 8.67% on average, with the maximum change of -9.78% in Case S-3 and the minimum change of -7.22% in Case L-3. The values of  $\overline{Nu}_{average} / Nu_0$  range from 3.3 to 5.1. The highest value is observed in the Case S-3, the blockage with the highest aspect ratio of the smaller area ratio cases, at Reynolds number of about 7,000. The lowest value is shown in Case L-1, the blockage with the lowest aspect ratio of the larger area ratio cases, at Reynolds number of about 17,000.

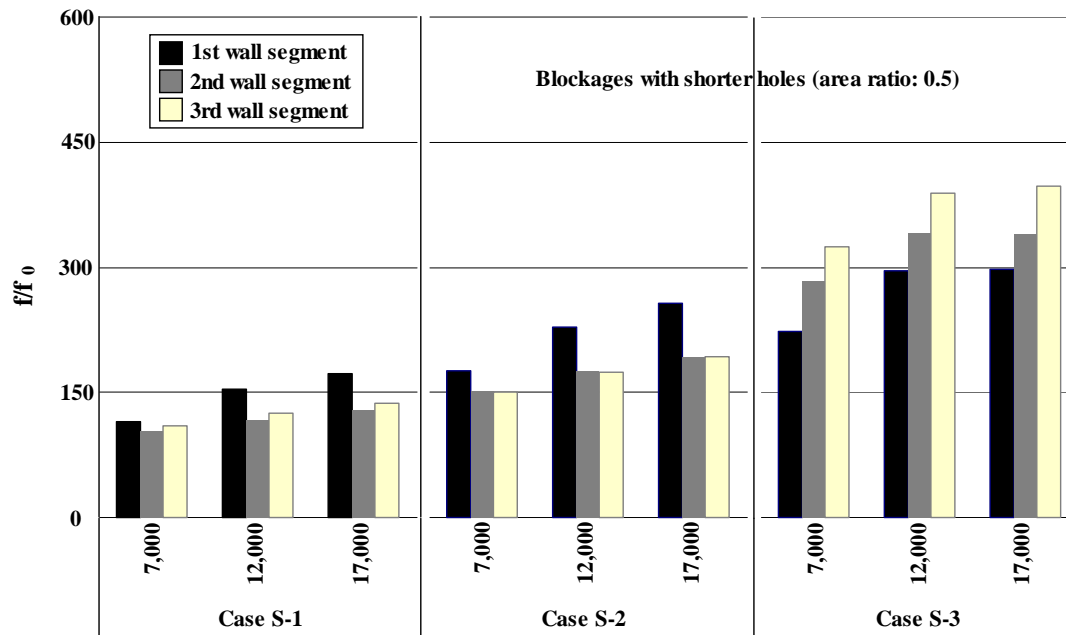
For the blockages with four or six holes, the differences in  $\overline{Nu}_{average} / Nu_0$  values between Case S-2 and S-3, and Case L-2 and L-3 at three different Reynolds numbers were insignificant comparing to those for the blockages with six or eight holes. Based on these results, average turbulent heat transfer enhancement effects of the blockages with four or six holes are similar to each other, whereas the heat transfer enhancement effect for the blockage with eight holes does not come up to the other two cases. The average value of average Nusselt number ratios on each segmented walls for the blockages with eight holes were, on average, about 11% and 12.5% less than those for the blockages with the four holes of the smaller area ratio, and for the larger area ratio cases, respectively.

The values of  $\overline{Nu}_{average} / Nu_0$  ranged from 4.1 to 5.1 for the blockages with the area ratio 0.5, and ranged from 3.3 to 4.1 for the blockages with the area ratio 0.6 as shown in Figure 6. This also means that the average heat transfer coefficients on the three segmented walls downstream of the blockages with elongated holes in the rectangular channel for fully developed turbulent flow are 4.1 ~ 5.1 and 3.3 ~ 4.1 times higher than those on the three segmented walls without blockages, i.e., smooth wall condition at the same Reynolds numbers. As speculated based on turbulent enhancement effect, the three kinds of blockages with the smaller area ratio showed the higher Nusselt number increment compared to those with the larger area ratio. This means that impinging and mixing effect yielding heat transfer enhancement is more significant in cases with the smaller area ratio.

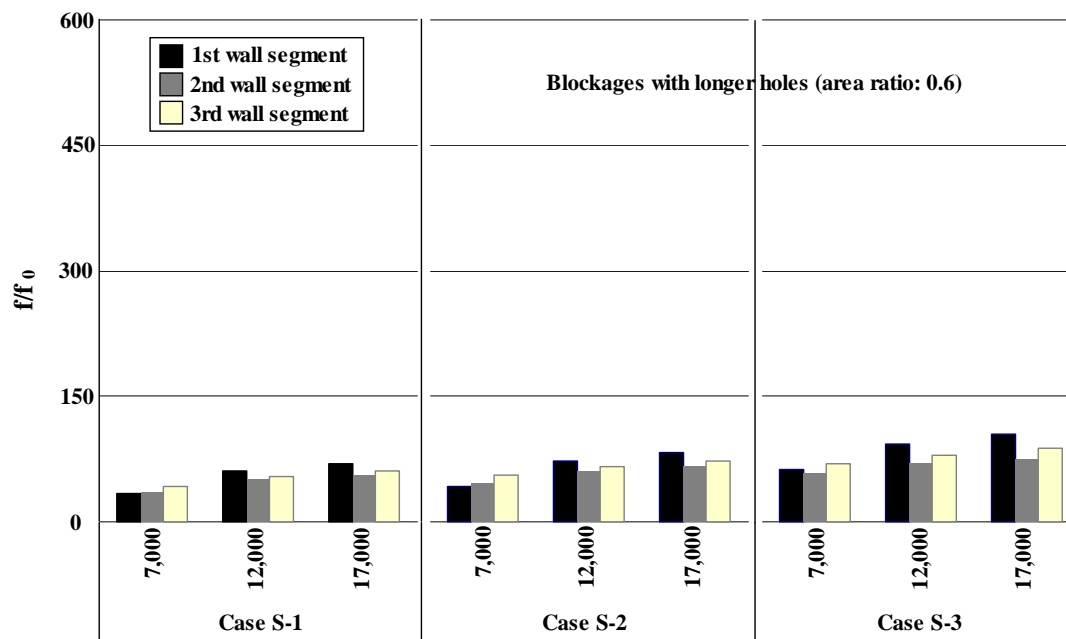
## B. Friction Factors

The friction factor can be calculated with the Equation C.4 using the pressure drops across two consecutive blockages – between the pressure taps in the first and the third row, between the pressure taps in the second and the fourth row, and between those in the third and the fifth row as shown in Figure 2.(b). The pressure drops across the blockages are larger than that in the flows across the channel without blockages at the same Reynolds number because blockages with elongated holes block about maximum 70% of the flow cross section of the rectangular channel. As shown in Figure 7, the blockages with the smaller area ratio in Cases S-1 through S-3 induce larger pressure drops than the blockages with the larger area ratio in Cases L-1 through L-3. As air flow rate increases, friction factor ratios also increase without exception for all cases. As the hole aspect ratio increases, friction factor ratios also increase from about 104 to about 397 for the blockages with shorter holes (smaller area ratio, 0.5), and from about 34 to about 104 for the blockages with longer holes (larger area ratio, 0.6). For the blockages with the shorter holes, as the aspect ratio of the holes increase from 1.55 to 2.88, the increase rates of corresponding friction factor ratios among the segments are from 72% to 272%, whereas for the blockages with the longer holes, just from 32% to 80% with the increase of aspect ratio from 1.88 to 3.41. The longer hole cases show significantly reduced increase rate of friction factor ratios as well as friction factors values themselves.

There are also variations of the values of the friction factor ratio among the three wall segments. For aspect ratio 2.88 with smaller area ratio, the friction factor values increase as the flow passes through blockages, but the other two cases show increment of the values only for the first segment with almost constant values for the second and third segments. As the number of holes increases, the difference in the value among the three segments decreases. For the area ratio 0.5, one of the three segments dominated friction factor ratio regardless of Reynolds number, whereas for area ratio 0.6, the ranks of segmental friction factor ratios varies depending on Reynolds number without any significant differences.



(a)



(b)

Fig. 7. Pressure drops across wall segments downstream of blockages relative to that for fully developed turbulent flow through a smooth channel without blockages.

### C. Thermal Performance

Thermal performance was evaluated as in Eq. C.6 using the average Nusselt number ratios on the three wall segments and the average of the friction factor ratios also for the three wall segments.

Figure 8 shows the average value of three segmental thermal performances of the blockages with the shorter and the longer holes. The blockages with larger area ratio (longer holes) outperform those with the shorter holes. TP values in cases with larger area ratio ranges from 0.84 to 1.11, while those in shorter hole cases ranges from 0.65 to 0.94. Although the shorter holes in the blockages cause more effective heat transfer enhancement than the longer holes in the blockages, they also induce much higher pressure drops across blockages. For the area ratio 0.5, as aspect ratio increases, thermal performances decrease in all cases, whereas for the area ratio 0.6, increasing aspect ratio does not guarantee better thermal performances within negligible differences in the values.



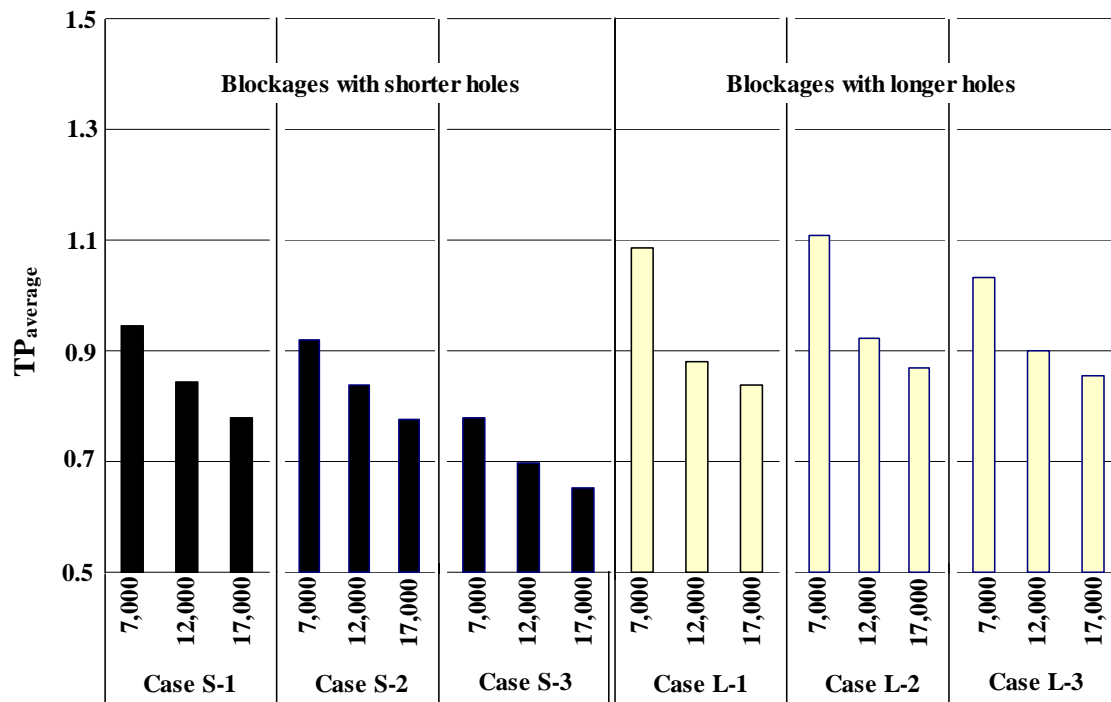


Fig. 8. Thermal performances of blockages with elongated holes – heat transfer enhancement per unit pumping power relative to that for fully developed flow through a smooth channel.

## CHAPTER IV

### RESULTS ANALYSIS

#### A. The Effect of Hole Area Ratio

Heat transfer enhancement effect occurs when the secondary flows mix with the main flows. There are two different kinds of secondary flows between two staggeringly arrayed consecutive blockages. One is formed when the coolant passes through the elongated holes as in rib turbulators for instance. The other is built when the coolant impinges onto the solid part between the two consecutive holes of blockages

On the basis of flow structure between two consecutive blockages, five heat transfer enhancement deciding factors can be speculated. The first factor is the number of impingement region. For instance, the blockages with eight holes have eight impingement regions. The second and the third are the total and partial areas of impingement region, respectively. Here, “partial area” means the region between two consecutive holes. The fourth and the fifth are the total and partial widths of reattachment region, respectively. Here, “partial width” means the width of one hole. The reason why the number of impingement region is important is because the blockages have limited size. For the impingement, area is important since the impingement region is vertical to the main flow direction, whereas for the reattachment region, only width is important since the reattachment region is formed depending on the width of holes.

These five heat transfer enhancement deciding factors are combined and decide final heat transfer enhancement effect. Using experimental results, the effects of these deciding factors can be confirmed numerically in terms of area and aspect ratios.

When the area ratio of blockages decreases from 0.6 to 0.5 between corresponding cases, the number of impingement region is maintained as four, six, and eight respectively and the partial and the total impingement area increase 67% but the partial and the total width of reattachment regions decrease about 15% for all pairs. Nusselt number ratios increase rates between corresponding cases are shown in Table II. Regardless of Reynolds numbers the increase rates are over 20%. This result shows that the increased partial and total impingement area enhances heat transfer significantly even though 15% decrease in the reattachment region weaken heat transfer from surface wall. Thus area ratio turned out to be the most effective parameter for heat transfer

enhancement in this study.

Table II. Hole area ratio effect - Nusselt number ratio increase rate

Reynolds numbers	Cases		
	L1→S1	L2→S2	L3→S3
7,000	25%	24%	24%
12,000	28%	29%	26%
17,000	24%	27%	20%
<b>Partial and total impingement area increase rate</b>	<b>65.8%↑</b>	<b>65.8%↑</b>	<b>65.8%↑</b>
<b>Partial and total width of reattachment region decrease rate</b>	<b>14.5%↓</b>	<b>15.4%↓</b>	<b>15.5%↓</b>

## B. The Effect of Hole Aspect Ratio

Aspect ratio analysis is more complicated than area ratio. For fixed area ratio, 0.5 or 0.6, aspect ratio increases ranging from 28% to 45% between eight holes and six holes cases or six holes and four holes cases as shown in Table III. Partial width of reattachment region and partial impingement area also increase but the number of impingement regions decreases from eight to four as the aspect ratio increases. The total width of reattachment region decreases slightly (about 3~4%) between cases under the consideration. Total impingement region area is definitely maintained as a constant, 0.5 or 0.6.

In this study at the low aspect ratio region, between eight and six hole cases, the Nusselt number ratio increase rate is over 10% regardless of Reynolds numbers for both types of blockages as shown in Table III. Hence, at this aspect ratio region, increased partial widths of reattachment region and impingement region area are dominant factors of heat transfer enhancement. But at high aspect ratio regions, between six holes and four holes cases, the Nusselt number ratio increase rate is under 4% and even -1% in the shorter hole types of blockages at highest Reynolds number of about 17,000. The reduced number of impingement region from six to four turned out to retard heat transfer from wall surface of a channel significantly.

Table III. Hole aspect ratio effect – Nusselt number ratio increase rate

Reynolds numbers	Cases			
	L1→L2	L2→L3	S1→S2	S2→S3
7,000	11%	1%	10%	2%
12,000	11%	4%	12%	1%
17,000	10%	4%	13%	-1%
Partial width of reattachment region	30% ↑	45% ↑	28% ↑	45% ↑
Partial impingement region area	33% ↑	50% ↑	33% ↑	50% ↑
Total width of reattachment region	2.8% ↓	3.1% ↓	3.9% ↓	3.2% ↓
Number of impingement region	8→6(25% ↓)	6→4(33% ↓)	8→6(25% ↓)	6→4(33% ↓)
Area ratio	0.6	0.6	0.5	0.5

## CHAPTER V

### SUMMARY AND CONCLUSIONS

#### A. Summary

Average convective heat transfer experiments were conducted using three copper plate heaters with total twenty one embedded thermocouples in 12:1 rectangular channel installed with four blockages with six different configurations of elongated holes. These experiments were conducted to measure and calculate average heat transfer enhancement, pressure drop and thermal performance on three segments of copper plates for fully developed turbulent flow. The results of experiments are summarized as follows:

1. Blockages with elongated holes enhance the heat transfer on three segments of rectangular channel wall downstream of the blockages, whereas they also cause pressure drops across two consecutive blockages. Therefore, heat transfer enhancement is beneficial but pressure drop is adverse compared to the heat transfer and pressure drop in case of fully developed turbulent flow at the same Reynolds number through smooth channel with same cross section.
2. The blockages with shorter holes (the smaller hole area ratio cases) enhance heat transfer better than those with longer holes (the larger hole area ratio cases) but they also yield significantly higher pressure drops than blockages with longer holes.
3. The blockages with longer holes in this study outperform the blockages with shorter holes.

#### B. Conclusions

For the experiments performed to study average heat transfer enhancement on rectangular channel wall, the conclusions are as follows:

1. The highest aspect ratio case of the smaller area ratio cases (Case S-3) showed the most effective heat transfer enhancement but the difference between Case S-3 and

S-2 was marginal.

2. For both types of blockages, shorter and longer hole types of blockages, as hole aspect ratio increases, the heat transfer on the wall segments is enhanced due to the increase in the reattached region and partial impingement area. Especially the effect of increased aspect ratio was significant at the low aspect ratio region between the lowest and the middle aspect ratio cases for both types of shorter and longer holes. In these cases, the flow reattachment and partial impingement area are the dominant factors determining the heat transfer on the channel wall.
3. The effect of increased aspect ratio at high aspect ratio region between the middle and the highest aspect ratio cases for both types of L and S was insignificant even though both the reattachment region and partial impingement area increase. The decrease in the number of recirculation regions blocking the flow by staggeringly installed blockages plays a major role in reducing heat transfer enhancement effect.
4. As the hole aspect ratio increases, the average pressure drop across blockages increases by the reduced number of penetrated regions which do not block the flow when the coolant passes through staggeringly placed four blockages. The blockages with the shorter holes yield higher pressure drop than those with the longer holes due to the increased blocking area.
5. The blockages with the longer holes outperform the blockages with the shorter holes due to the significant pressure drops caused by the blockages with shorter holes. The Case L-2 has the highest TP value of all cases. The Case S-2 can be an alternative to the Case L-2 from the heat transfer enhancement point of view if the pressure drop is acceptable.

In this study, experiments to measure average heat transfer enhancement were performed for blockages with only elongated holes for the purpose of application of gas turbine trailing edge or middle portion internal cooling. Based on the results, Case L-2 is the best option based on TP value, but Case S-2 can be an alternative to Case L-2 if the level of penalty from pressure drop is acceptable.

For the optimized area and aspect ratios of the holes in blockages, additional

parametric studies are needed. By impinging and recirculation effects on upstream and downstream the surfaces of blockages, heat transfer on the surfaces of blockages made of the same material to the channel wall need to be measured and considered for more effective cooling by local heat transfer measurement method such as IR or naphthalene sublimation. This is because a substantial amount of heat may be conducted from the pressure and suction walls to the blockages.



## REFERENCES

- [1] Takeishi, K., "Heat transfer research in high temperature industrial gas turbines," in *Proc. International Symposium on Heat Transfer in Turbomachinery*, Marathon, Greece, 1992
- [2] Han, J.C. and Park, J.S., "Developing heat transfer in rectangular channels with rib turbulators," *Int. J. Heat Mass Transfer*, vol. 31, pp. 183-195, 1987
- [3] Han, J.C. and Zhang, Y.M., "High performance heat transfer ducts with parallel broken and V-Shaped broken ribs," *Int. J. Heat Mass Transfer*, vol. 35, pp. 513-523, 1992
- [4] VanFossen, G.J., "Heat transfer coefficient for staggered arrays of short pin fins," *ASME Journal of Engineering for Power*, vol. 104, pp. 268-274, 1982
- [5] Taslim, M.E. and Spring, S.D., "Effects of turbulator profile and spacing on heat transfer and friction in a channel," *AIAA Journal of Thermodynamics and Heat Transfer*, vol. 8, pp. 555-562, 1994.
- [6] Kukreja, R.T. and Lau, S.C., "Distributions of local heat transfer coefficient on surfaces with solid and perforated ribs," *Journal of Enhanced Heat Transfer*, vol. 5, pp. 9-21, 1998
- [7] Kukreja, R.T., Lau, S.C. and McMillan, R.D., "Local heat(mass) transfer distribution in a square channel with full and V-shaped ribs," *Int. J. Heat Mass Transfer*, vol. 36, pp. 2013-2020, 1993.
- [8] Lau, S.C., Kim, Y.S., and Han, J.C., "Local endwall heat/mass transfer distributions in pin fin channels," *J. Thermophysics*, vol. 1, pp. 365-372, 1987.
- [9] Lau, S.C., Cervantes, J., Han, J.C., Rudolph, R.J., and Flannery, K., "Measurements of wall heat(mass) transfer for flow through blockages with round and square holes in a wide rectangular channel," *Int J. Heat mass Transfer*, vol. 46, pp. 3991-4001,

2003.

- [10] Han, J.C., Dutta, S., and Ekkad, S.V., *Gas turbine heat transfer and cooling technology*, New York, NY: Taylor and Francis, 2000.
- [11] Lau, S.C., Enhanced internal cooling of gas turbine airfoil, in Sunden, B., and Faghri, M., Eds., *Heat Transfer in Gas Turbines*, Southampton, UK: WIT Press, 2001.
- [12] Lau, S.C., Kukreja, R.T., and McMillan, R.D, "Effects of V-shaped rib arrays on turbulent heat transfer and friction of fully developed flow in a square channel," *Int. J. Heat Mass Transfer*, vol. 34, pp. 1605-1616, 1991.
- [13] Buchlin, J.M., "Convective heat transfer in a channel with perforated ribs," *Int. J. Thermal Sciences*, vol. 41, pp. 332-340, 2002.
- [14] Bailey, J.C. and Bunker, R.S., "Heat transfer and friction in channels with very high blockages 45 degree staggered turbulators," in *Proc. ASME Turbo Expo 2003*, Atlanta, GA, 2003.
- [15] Armstrong, J. and Winstanley, D., "A review of staggered array pin fin heat transfer for turbine cooling applications," *Transactions of ASME*, vol. 110, pp. 94-103, 1988.
- [16] Metzger, D.E., Berry, R.A., and Bronson, J.P., "Developing heat transfer in rectangular ducts with arrays of short pin fins," *ASME Paper No. 81-WA/HT-6*, 1981.
- [17] Metzger, D.E. and Haley, S.W., "Heat transfer experiments and flow visualization for arrays of short pin fins," *ASME Paper No. 82-GT-138*, 1982.
- [18] Metzger, D.E., Fan, Z.X., and Shepard, W.B., "Pressure loss and heat transfer through multiple rows of short pin fins," *Heat Transfer*, 1982, vol. 3, U. Grigull et al., Eds., Washington, DC, pp. 137-142: Hemisphere, 1982.
- [19] Metzger, D.E., Shepard, W.B., and Haley, S.W., "Row resolved heat transfer

variations in pin fin arrays including effects of non-uniform arrays and flow convergence,” *ASME Paper No. 86-GT-132*, 1986.\

- [20] Zukauskas, A.A., “Heat transfer from tubes in cross flow,” *Adv. in Heat Transfer*, vol. 8, pp. 116-133, 1972.
- [21] Brigham, B.A. and VanFossen, G.J., “Length-to-diameter ratio and row number effects in short pin fin heat transfer,” *ASME J. Engineering for Gas Turbines and Power*, vol. 106, pp. 241-245, 1984.
- [22] Lau, S.C., Han, J.C., and Kim, Y.S., “Turbulent heat transfer and friction in pin fin channels with lateral flow ejection,” *ASME J. Heat Transfer*, vol. 111, pp. 51-58, 1989.
- [23] Lau, S.C., and Han, J.C., Batten, T., “Heat transfer, pressure drop, and mass flow rate in pin fin channels with long and short trailing edge ejection holes,” *ASME J. Turbomachinery*, vol. 111, pp. 116-123, 1989.
- [24] Lau, S.C., McMillan, R.D., and Kukreja, R.T., “Segmental heat transfer in a pin fin channel with ejection holes,” *Int. J. Heat Transfer*, vol. 35, pp. 1407-1417, 1992.
- [25] Ligrani, P.M. and Mahmood, G.I., “Local heat transfer and flow structure on and above a dimpled surface in a channel,” *Transactions of ASME*, vol. 123, pp. 115-123, 2001.
- [26] Ligrani, P.M. and Mahmood, G.I., “Heat transfer in a dimpled channel: combined influences of aspect ratio, temperature ratio, Reynolds number, and flow structure,” *Int. J. Heat and Mass Transfer*, vol. 45, pp. 2011-2020, 2002.
- [27] Ligrani, P.M. and Burgess, N.K., “Effects of dimple depth on channel Nusselt numbers and friction factors ,” *ASME J. Heat Transfer*, vol. 127, pp. 839-847, 2005.
- [28] Moon, S.W. and Lau, S.C., “Heat transfer between blockages with holes in a rectangular channel,” *ASME J. Heat transfer*, vol. 125, pp. 587-594, 2003.

- [29] Coleman, H.W. and Steele, W.G., *Experimentation and Uncertainty Analysis for Engineers*, New York, NY: John Wiley & Sons, 1989.

## APPENDIX A

### CALCULATED DATA FOR HEAT TRANSFER MEASUREMENT

Table IV. Average Nusselt numbers obtained from heat transfer measurement

Case	$Re$	$\overline{Nu}$			$Nu_0$	$\overline{Nu}_{average}/Nu_0$
		1 <sup>st</sup> segment	2 <sup>nd</sup> segment	3 <sup>rd</sup> segment		
S-1	7,000	107	103	92	22.3	4.52
	12,000	153	149	138	34.3	4.28
	17,000	192	188	178	45.5	4.09
S-2	7,000	108	113	112	22.3	4.98
	12,000	158	170	168	34.3	4.82
	17,000	199	218	215	45.6	4.62
S-3	7,000	109	114	119	22.5	5.06
	12,000	157	169	178	34.5	4.87
	17,000	194	209	221	45.6	4.56
L-1	7,000	87	81	75	22.4	3.62
	12,000	122	115	109	34.4	3.35
	17,000	158	151	144	45.7	3.30
L-2	7,000	93	92	84	22.3	4.02
	12,000	132	129	123	34.4	3.73
	17,000	169	167	161	45.6	3.63
L-3	7,000	92	94	88	22.3	4.08
	12,000	132	136	130	34.3	3.87
	17,000	171	176	171	45.6	3.79

Table V. Segmental friction factors obtained with heat transfer measurement

Case	$Re$	$f$			$f_0$	$f_{average}/f_0$
		1 <sup>st</sup> segment	2 <sup>nd</sup> segment	3 <sup>rd</sup> segment		
S-1	7,000	3.98	3.61	3.81	0.0348	109
	12,000	4.61	3.49	3.75	0.0299	132
	17,000	4.69	3.49	3.70	0.0272	146
S-2	7,000	6.09	5.31	5.24	0.0348	160
	12,000	6.83	5.26	5.22	0.0299	193
	17,000	6.96	5.23	5.23	0.0271	214
S-3	7,000	7.74	9.86	11.26	0.0347	277
	12,000	8.82	10.17	11.61	0.0298	342
	17,000	8.08	9.23	10.77	0.0271	345
L-1	7,000	1.19	1.22	1.48	0.0347	37
	12,000	1.79	1.54	1.63	0.0299	55
	17,000	1.87	1.52	1.63	0.0271	62
L-2	7,000	1.49	1.59	1.96	0.0348	48
	12,000	2.17	1.81	1.96	0.0299	66
	17,000	2.23	1.80	1.97	0.0271	74
L-3	7,000	2.15	1.98	2.38	0.0348	62
	12,000	2.77	2.07	2.37	0.0299	80
	17,000	2.83	2.00	2.38	0.0271	89

Table VI. Thermal performances obtained with heat transfer measurement

Case	$Re$	$TP$			$\overline{TP}$
		1 <sup>st</sup> segment	2 <sup>nd</sup> segment	3 <sup>rd</sup> segment	
S-1	7,000	0.992	0.983	0.859	0.945
	12,000	0.834	0.888	0.806	0.843
	17,000	0.759	0.819	0.762	0.780
S-2	7,000	0.869	0.948	0.942	0.919
	12,000	0.752	0.884	0.877	0.837
	17,000	0.687	0.827	0.816	0.777
S-3	7,000	0.795	0.769	0.769	0.778
	12,000	0.683	0.699	0.707	0.696
	17,000	0.638	0.656	0.660	0.651
L-1	7,000	1.195	1.102	0.963	1.087
	12,000	0.907	0.896	0.835	0.879
	17,000	0.843	0.861	0.807	0.837
L-2	7,000	1.191	1.153	0.985	1.110
	12,000	0.919	0.960	0.887	0.922
	17,000	0.852	0.906	0.846	0.868
L-3	7,000	1.039	1.092	0.963	1.031
	12,000	0.851	0.965	0.883	0.900
	17,000	0.798	0.922	0.843	0.854

## APPENDIX B

### EXPERIMENTAL DATA FOR HEAT TRANSFER MEASUREMENT

Table VII. Voltage and current readings of Type S for power consumption measurement

Unit – Voltage: V, Current I: A

Re	Case S-1						Case S-2					
	V			I			V			I		
	1st plate	2nd plate	3rd plate	1st plate	2nd plate	3rd plate	1st plate	2nd plate	3rd plate	1st plate	2nd plate	3rd plate
7,000	3.82E+01	3.61E+01	3.50E+01	6.91E-01	6.61E-01	6.19E-01	3.77E+01	3.73E+01	3.72E+01	7.00E-01	6.90E-01	6.83E-01
	3.82E+01	3.61E+01	3.50E+01	6.91E-01	6.61E-01	6.19E-01	3.77E+01	3.73E+01	3.72E+01	7.01E-01	6.90E-01	6.83E-01
	3.82E+01	3.61E+01	3.50E+01	6.91E-01	6.61E-01	6.19E-01	3.77E+01	3.73E+01	3.72E+01	7.00E-01	6.90E-01	6.83E-01
	3.82E+01	3.61E+01	3.50E+01	6.91E-01	6.61E-01	6.19E-01	3.77E+01	3.73E+01	3.72E+01	7.01E-01	6.90E-01	6.83E-01
	3.82E+01	3.61E+01	3.50E+01	6.91E-01	6.61E-01	6.19E-01	3.77E+01	3.73E+01	3.72E+01	7.01E-01	6.90E-01	6.83E-01
12,000	4.51E+01	4.30E+01	4.22E+01	8.08E-01	7.83E-01	7.45E-01	4.51E+01	4.52E+01	4.51E+01	8.38E-01	8.50E-01	8.34E-01
	4.50E+01	4.30E+01	4.21E+01	8.09E-01	7.83E-01	7.46E-01	4.51E+01	4.53E+01	4.52E+01	8.38E-01	8.51E-01	8.35E-01
	4.51E+01	4.30E+01	4.21E+01	8.09E-01	7.83E-01	7.45E-01	4.51E+01	4.52E+01	4.51E+01	8.38E-01	8.50E-01	8.34E-01
	4.49E+01	4.30E+01	4.22E+01	8.09E-01	7.83E-01	7.46E-01	4.51E+01	4.53E+01	4.52E+01	8.38E-01	8.51E-01	8.35E-01
	4.50E+01	4.30E+01	4.21E+01	8.08E-01	7.83E-01	7.45E-01	4.51E+01	4.52E+01	4.51E+01	8.38E-01	8.50E-01	8.34E-01
17,000	5.02E+01	4.83E+01	4.72E+01	8.91E-01	8.69E-01	8.42E-01	5.10E+01	5.14E+01	5.14E+01	9.30E-01	9.62E-01	9.37E-01
	5.03E+01	4.83E+01	4.72E+01	8.91E-01	8.69E-01	8.42E-01	5.10E+01	5.14E+01	5.14E+01	9.30E-01	9.62E-01	9.37E-01
	5.02E+01	4.83E+01	4.72E+01	8.91E-01	8.69E-01	8.42E-01	5.10E+01	5.14E+01	5.14E+01	9.30E-01	9.62E-01	9.37E-01
	5.02E+01	4.83E+01	4.72E+01	8.91E-01	8.69E-01	8.42E-01	5.10E+01	5.14E+01	5.14E+01	9.30E-01	9.62E-01	9.37E-01
	5.02E+01	4.83E+01	4.72E+01	8.91E-01	8.69E-01	8.42E-01	5.10E+01	5.14E+01	5.14E+01	9.30E-01	9.62E-01	9.37E-01
Re	Case S-3											
	V			I								
	1st plate	2nd plate	3rd plate	1st plate	2nd plate	3rd plate						
7,000	3.95E+01	3.91E+01	3.99E+01	7.34E-01	7.29E-01	7.39E-01						
	3.96E+01	3.91E+01	3.98E+01	7.35E-01	7.30E-01	7.39E-01						
	3.95E+01	3.91E+01	3.99E+01	7.34E-01	7.29E-01	7.39E-01						
	3.96E+01	3.91E+01	3.98E+01	7.35E-01	7.30E-01	7.39E-01						
	3.95E+01	3.91E+01	3.99E+01	7.34E-01	7.29E-01	7.39E-01						
12,000	4.67E+01	4.70E+01	4.78E+01	8.65E-01	8.74E-01	8.92E-01						
	4.67E+01	4.70E+01	4.79E+01	8.65E-01	8.75E-01	8.91E-01						
	4.67E+01	4.70E+01	4.78E+01	8.65E-01	8.74E-01	8.92E-01						
	4.67E+01	4.70E+01	4.78E+01	8.65E-01	8.75E-01	8.93E-01						
	4.67E+01	4.70E+01	4.78E+01	8.65E-01	8.74E-01	8.92E-01						
17,000	5.02E+01	5.08E+01	5.18E+01	9.29E-01	9.43E-01	9.64E-01						
	5.02E+01	5.08E+01	5.17E+01	9.29E-01	9.42E-01	9.63E-01						
	5.02E+01	5.08E+01	5.17E+01	9.29E-01	9.42E-01	9.64E-01						
	5.02E+01	5.08E+01	5.18E+01	9.29E-01	9.43E-01	9.64E-01						
	5.02E+01	5.08E+01	5.17E+01	9.29E-01	9.42E-01	9.63E-01						



Table VIII. Voltage and current readings of Type L for power consumption measurement

Unit – Voltage: V, Current I: A

Re	Case L-1						Case L-2					
	V			I			V			I		
	1st plate	2nd plate	3rd plate	1st plate	2nd plate	3rd plate	1st plate	2nd plate	3rd plate	1st plate	2nd plate	3rd plate
7,000	3.47E+01	3.25E+01	3.22E+01	6.46E-01	6.10E-01	5.91E-01	3.50E+01	3.35E+01	3.29E+01	6.65E-01	6.46E-01	6.17E-01
	3.47E+01	3.25E+01	3.22E+01	6.47E-01	6.10E-01	5.91E-01	3.50E+01	3.35E+01	3.29E+01	6.65E-01	6.47E-01	6.18E-01
	3.47E+01	3.25E+01	3.22E+01	6.46E-01	6.10E-01	5.91E-01	3.50E+01	3.35E+01	3.29E+01	6.65E-01	6.46E-01	6.17E-01
	3.47E+01	3.25E+01	3.22E+01	6.47E-01	6.10E-01	5.91E-01	3.50E+01	3.35E+01	3.29E+01	6.65E-01	6.47E-01	6.17E-01
	3.47E+01	3.25E+01	3.22E+01	6.46E-01	6.10E-01	5.91E-01	3.50E+01	3.35E+01	3.29E+01	6.65E-01	6.46E-01	6.18E-01
12,000	4.06E+01	3.82E+01	3.81E+01	7.49E-01	7.18E-01	6.96E-01	4.12E+01	3.94E+01	3.93E+01	7.75E-01	7.58E-01	7.28E-01
	4.06E+01	3.82E+01	3.81E+01	7.50E-01	7.18E-01	6.96E-01	4.11E+01	3.94E+01	3.94E+01	7.75E-01	7.59E-01	7.29E-01
	4.06E+01	3.82E+01	3.81E+01	7.50E-01	7.18E-01	6.96E-01	4.12E+01	3.94E+01	3.93E+01	7.74E-01	7.58E-01	7.28E-01
	4.06E+01	3.82E+01	3.81E+01	7.50E-01	7.18E-01	6.96E-01	4.11E+01	3.94E+01	3.94E+01	7.75E-01	7.59E-01	7.29E-01
	4.06E+01	3.82E+01	3.81E+01	7.50E-01	7.18E-01	6.96E-01	4.11E+01	3.94E+01	3.93E+01	7.74E-01	7.58E-01	7.28E-01
17,000	4.56E+01	4.34E+01	4.33E+01	8.45E-01	8.15E-01	7.90E-01	4.62E+01	4.47E+01	4.45E+01	8.68E-01	8.52E-01	8.25E-01
	4.56E+01	4.34E+01	4.33E+01	8.45E-01	8.15E-01	7.90E-01	4.61E+01	4.47E+01	4.46E+01	8.67E-01	8.52E-01	8.26E-01
	4.56E+01	4.34E+01	4.33E+01	8.45E-01	8.15E-01	7.90E-01	4.62E+01	4.47E+01	4.45E+01	8.68E-01	8.52E-01	8.25E-01
	4.56E+01	4.34E+01	4.33E+01	8.45E-01	8.15E-01	7.90E-01	4.61E+01	4.47E+01	4.46E+01	8.67E-01	8.52E-01	8.26E-01
	4.56E+01	4.34E+01	4.33E+01	8.45E-01	8.15E-01	7.90E-01	4.62E+01	4.47E+01	4.45E+01	8.68E-01	8.52E-01	8.25E-01
Re	Case L-3											
	V			I								
	1st plate	2nd plate	3rd plate	1st plate	2nd plate	3rd plate						
7,000	3.56E+01	3.51E+01	3.45E+01	6.44E-01	6.26E-01	6.10E-01						
	3.56E+01	3.51E+01	3.45E+01	6.45E-01	6.26E-01	6.11E-01						
	3.54E+01	3.51E+01	3.45E+01	6.44E-01	6.26E-01	6.10E-01						
	3.56E+01	3.51E+01	3.45E+01	6.45E-01	6.26E-01	6.11E-01						
	3.56E+01	3.51E+01	3.45E+01	6.44E-01	6.26E-01	6.11E-01						
12,000	4.20E+01	4.16E+01	4.12E+01	7.63E-01	7.53E-01	7.31E-01						
	4.20E+01	4.16E+01	4.13E+01	7.63E-01	7.53E-01	7.32E-01						
	4.20E+01	4.16E+01	4.12E+01	7.63E-01	7.53E-01	7.31E-01						
	4.20E+01	4.16E+01	4.13E+01	7.63E-01	7.53E-01	7.32E-01						
	4.20E+01	4.16E+01	4.12E+01	7.63E-01	7.53E-01	7.31E-01						
17,000	4.70E+01	4.67E+01	4.65E+01	8.61E-01	8.53E-01	8.31E-01						
	4.70E+01	4.68E+01	4.65E+01	8.62E-01	8.54E-01	8.31E-01						
	4.70E+01	4.67E+01	4.65E+01	8.61E-01	8.53E-01	8.31E-01						
	4.70E+01	4.68E+01	4.65E+01	8.62E-01	8.54E-01	8.31E-01						
	4.70E+01	4.67E+01	4.65E+01	8.62E-01	8.53E-01	8.31E-01						

Table IX. Voltage readings of Case S-1 for pressure drop measurement

Unit – Voltage: V

Re	V for Pressure								
	V <sub>P1</sub>	V <sub>P2</sub>	V <sub>P3</sub>	V <sub>P4</sub>	V <sub>P5</sub>	V <sub>P6</sub>	V <sub>P7</sub>	V <sub>P8</sub>	V <sub>P9</sub>
	1st pressure drop			2nd pressure drop			3rd pressure drop		
7,000	9.500E-03	9.500E-03	9.700E-03	1.710E-02	1.770E-02	1.800E-02	2.290E-02	2.310E-02	2.430E-02
	9.500E-03	9.500E-03	9.700E-03	1.720E-02	1.780E-02	1.820E-02	2.300E-02	2.310E-02	2.410E-02
	9.500E-03	9.500E-03	9.700E-03	1.710E-02	1.780E-02	1.810E-02	2.290E-02	2.300E-02	2.420E-02
	9.500E-03	9.500E-03	9.700E-03	1.710E-02	1.760E-02	1.790E-02	2.310E-02	2.310E-02	2.410E-02
	9.500E-03	9.500E-03	9.700E-03	1.720E-02	1.770E-02	1.790E-02	2.310E-02	2.320E-02	2.420E-02
12,000	1.600E-02	1.580E-02	1.650E-02	4.550E-02	4.630E-02	4.740E-02	6.150E-02	6.130E-02	6.530E-02
	1.600E-02	1.570E-02	1.660E-02	4.570E-02	4.670E-02	4.730E-02	6.120E-02	6.120E-02	6.590E-02
	1.600E-02	1.580E-02	1.660E-02	4.570E-02	4.670E-02	4.720E-02	6.150E-02	6.120E-02	6.540E-02
	1.600E-02	1.580E-02	1.660E-02	4.530E-02	4.690E-02	4.710E-02	6.130E-02	6.130E-02	6.510E-02
	1.600E-02	1.580E-02	1.670E-02	4.510E-02	4.670E-02	4.740E-02	6.150E-02	6.140E-02	6.530E-02
17,000	2.810E-02	2.770E-02	2.900E-02	9.070E-02	9.130E-02	9.540E-02	1.223E-01	1.228E-01	1.321E-01
	2.810E-02	2.760E-02	2.900E-02	9.190E-02	9.180E-02	9.510E-02	1.237E-01	1.225E-01	1.325E-01
	2.820E-02	2.760E-02	2.890E-02	9.110E-02	9.190E-02	9.580E-02	1.234E-01	1.226E-01	1.318E-01
	2.810E-02	2.760E-02	2.890E-02	9.110E-02	9.220E-02	9.570E-02	1.227E-01	1.229E-01	1.337E-01
	2.810E-02	2.760E-02	2.900E-02	9.100E-02	9.180E-02	9.520E-02	1.228E-01	1.230E-01	1.321E-01
Re	V <sub>P10</sub>	V <sub>P11</sub>	V <sub>P12</sub>	V <sub>P13</sub>	V <sub>P14</sub>	V <sub>P15</sub>			
	4th pressure drop			5th pressure drop					
7,000	2.990E-02	3.030E-02	3.030E-02	3.660E-02	3.660E-02	3.670E-02			
	2.990E-02	3.020E-02	3.040E-02	3.680E-02	3.670E-02	3.660E-02			
	3.020E-02	3.030E-02	3.030E-02	3.680E-02	3.660E-02	3.670E-02			
	3.000E-02	3.030E-02	3.030E-02	3.680E-02	3.680E-02	3.670E-02			
	3.000E-02	3.030E-02	3.030E-02	3.670E-02	3.670E-02	3.700E-02			
12,000	8.220E-02	8.200E-02	8.140E-02	9.960E-02	1.001E-01	1.002E-01			
	8.230E-02	8.200E-02	8.150E-02	1.002E-01	1.007E-01	1.006E-01			
	8.170E-02	8.180E-02	8.130E-02	1.003E-01	1.006E-01	1.013E-01			
	8.130E-02	8.200E-02	8.180E-02	1.007E-01	1.012E-01	1.012E-01			
	8.170E-02	8.200E-02	8.170E-02	1.009E-01	1.008E-01	1.007E-01			
17,000	1.644E-01	1.648E-01	1.670E-01	2.025E-01	2.031E-01	2.030E-01			
	1.638E-01	1.660E-01	1.665E-01	2.039E-01	2.032E-01	2.030E-01			
	1.645E-01	1.664E-01	1.664E-01	2.036E-01	2.035E-01	2.025E-01			
	1.643E-01	1.657E-01	1.662E-01	2.037E-01	2.035E-01	2.029E-01			
	1.646E-01	1.652E-01	1.669E-01	2.035E-01	2.033E-01	2.035E-01			

Table X. Voltage readings of Case S-2 for pressure drop measurement

Unit – Voltage: V

Re	V for Pressure								
	V <sub>P1</sub>	V <sub>P2</sub>	V <sub>P3</sub>	V <sub>P4</sub>	V <sub>P5</sub>	V <sub>P6</sub>	V <sub>P7</sub>	V <sub>P8</sub>	V <sub>P9</sub>
	1st pressure drop			2nd pressure drop			3rd pressure drop		
7,000	1.150E-02	1.140E-02	1.180E-02	2.320E-02	2.440E-02	2.170E-02	3.260E-02	3.060E-02	3.490E-02
	1.150E-02	1.140E-02	1.190E-02	2.300E-02	2.420E-02	2.170E-02	3.260E-02	3.090E-02	3.510E-02
	1.150E-02	1.140E-02	1.190E-02	2.330E-02	2.430E-02	2.140E-02	3.240E-02	3.080E-02	3.510E-02
	1.150E-02	1.140E-02	1.190E-02	2.320E-02	2.460E-02	2.160E-02	3.260E-02	3.090E-02	3.550E-02
	1.150E-02	1.140E-02	1.190E-02	2.310E-02	2.450E-02	2.140E-02	3.230E-02	3.070E-02	3.510E-02
12,000	1.640E-02	1.620E-02	1.770E-02	5.740E-02	6.100E-02	5.280E-02	8.390E-02	7.910E-02	9.270E-02
	1.640E-02	1.620E-02	1.760E-02	5.770E-02	6.100E-02	5.280E-02	8.370E-02	8.000E-02	9.380E-02
	1.640E-02	1.620E-02	1.760E-02	5.770E-02	6.110E-02	5.340E-02	8.390E-02	7.910E-02	9.400E-02
	1.650E-02	1.620E-02	1.770E-02	5.770E-02	6.090E-02	5.300E-02	8.360E-02	7.930E-02	9.380E-02
	1.640E-02	1.600E-02	1.770E-02	5.770E-02	6.070E-02	5.310E-02	8.400E-02	8.020E-02	9.460E-02
17,000	2.660E-02	2.570E-02	2.930E-02	1.160E-01	1.215E-01	1.055E-01	1.680E-01	1.588E-01	1.898E-01
	2.660E-02	2.570E-02	2.930E-02	1.162E-01	1.208E-01	1.045E-01	1.677E-01	1.599E-01	1.887E-01
	2.660E-02	2.580E-02	2.930E-02	1.157E-01	1.212E-01	1.047E-01	1.688E-01	1.593E-01	1.882E-01
	2.670E-02	2.570E-02	2.930E-02	1.160E-01	1.205E-01	1.049E-01	1.702E-01	1.586E-01	1.881E-01
	2.660E-02	2.570E-02	2.930E-02	1.159E-01	1.218E-01	1.046E-01	1.654E-01	1.590E-01	1.890E-01
Re	V <sub>P10</sub>	V <sub>P11</sub>	V <sub>P12</sub>	V <sub>P13</sub>	V <sub>P14</sub>	V <sub>P15</sub>			
	4th pressure drop			5th pressure drop					
7,000	4.180E-02	4.250E-02	4.050E-02	5.080E-02	5.000E-02	5.240E-02			
	4.190E-02	4.230E-02	4.060E-02	5.110E-02	5.000E-02	5.270E-02			
	4.220E-02	4.210E-02	4.040E-02	5.090E-02	4.950E-02	5.260E-02			
	4.190E-02	4.230E-02	4.030E-02	5.080E-02	4.980E-02	5.210E-02			
	4.190E-02	4.200E-02	4.040E-02	5.110E-02	4.970E-02	5.210E-02			
12,000	1.111E-01	1.121E-01	1.089E-01	1.381E-01	1.370E-01	1.402E-01			
	1.116E-01	1.116E-01	1.098E-01	1.393E-01	1.359E-01	1.417E-01			
	1.113E-01	1.112E-01	1.078E-01	1.384E-01	1.352E-01	1.403E-01			
	1.106E-01	1.113E-01	1.071E-01	1.392E-01	1.347E-01	1.413E-01			
	1.107E-01	1.109E-01	1.083E-01	1.396E-01	1.344E-01	1.412E-01			
17,000	2.237E-01	2.246E-01	2.183E-01	2.792E-01	2.739E-01	2.867E-01			
	2.254E-01	2.245E-01	2.199E-01	2.802E-01	2.736E-01	2.898E-01			
	2.247E-01	2.251E-01	2.174E-01	2.805E-01	2.741E-01	2.872E-01			
	2.238E-01	2.265E-01	2.188E-01	2.802E-01	2.750E-01	2.874E-01			
	2.252E-01	2.261E-01	2.192E-01	2.797E-01	2.734E-01	2.893E-01			

Table XI. Voltage readings of Case S-3 for pressure drop measurement

Unit – Voltage: V

Re	V for Pressure								
	V <sub>P1</sub>	V <sub>P2</sub>	V <sub>P3</sub>	V <sub>P4</sub>	V <sub>P5</sub>	V <sub>P6</sub>	V <sub>P7</sub>	V <sub>P8</sub>	V <sub>P9</sub>
	1st pressure drop			2nd pressure drop			3rd pressure drop		
7,000	8.100E-03	7.900E-03	8.600E-03	2.240E-02	2.330E-02	1.470E-02	3.500E-02	2.980E-02	4.020E-02
	8.100E-03	7.900E-03	8.600E-03	2.250E-02	2.340E-02	1.480E-02	3.520E-02	2.960E-02	4.040E-02
	8.100E-03	7.900E-03	8.600E-03	2.260E-02	2.340E-02	1.480E-02	3.520E-02	2.970E-02	4.040E-02
	8.100E-03	7.900E-03	8.600E-03	2.240E-02	2.360E-02	1.480E-02	3.550E-02	2.980E-02	4.040E-02
	8.100E-03	7.900E-03	8.600E-03	2.250E-02	2.340E-02	1.470E-02	3.530E-02	2.970E-02	4.030E-02
12,000	1.350E-02	1.270E-02	1.600E-02	6.590E-02	6.770E-02	4.180E-02	1.026E-01	8.690E-02	1.201E-01
	1.350E-02	1.250E-02	1.600E-02	6.610E-02	6.790E-02	4.150E-02	1.024E-01	8.670E-02	1.198E-01
	1.340E-02	1.260E-02	1.600E-02	6.540E-02	6.780E-02	4.130E-02	1.031E-01	8.630E-02	1.198E-01
	1.350E-02	1.280E-02	1.600E-02	6.590E-02	6.740E-02	4.160E-02	1.028E-01	8.640E-02	1.193E-01
	1.350E-02	1.270E-02	1.600E-02	6.530E-02	6.780E-02	4.140E-02	1.024E-01	8.620E-02	1.192E-01
17,000	2.300E-02	2.130E-02	2.840E-02	1.237E-01	1.276E-01	7.720E-02	1.912E-01	1.613E-01	2.239E-01
	2.300E-02	2.120E-02	2.840E-02	1.235E-01	1.270E-01	7.650E-02	1.916E-01	1.608E-01	2.237E-01
	2.300E-02	2.120E-02	2.840E-02	1.235E-01	1.276E-01	7.700E-02	1.910E-01	1.602E-01	2.237E-01
	2.300E-02	2.130E-02	2.840E-02	1.235E-01	1.272E-01	7.680E-02	1.914E-01	1.602E-01	2.251E-01
	2.300E-02	2.110E-02	2.850E-02	1.237E-01	1.275E-01	7.660E-02	1.912E-01	1.606E-01	2.240E-01
Re	V <sub>P10</sub>	V <sub>P11</sub>	V <sub>P12</sub>	V <sub>P13</sub>	V <sub>P14</sub>	V <sub>P15</sub>			
	4th pressure drop			5th pressure drop					
7,000	5.720E-02	5.890E-02	4.800E-02	7.720E-02	7.210E-02	7.290E-02			
	5.750E-02	5.810E-02	4.790E-02	7.660E-02	7.350E-02	7.280E-02			
	5.770E-02	5.800E-02	4.800E-02	7.620E-02	7.290E-02	7.280E-02			
	5.740E-02	5.830E-02	4.780E-02	7.750E-02	7.280E-02	7.280E-02			
	5.720E-02	5.790E-02	4.770E-02	7.750E-02	7.280E-02	7.320E-02			
12,000	1.698E-01	1.710E-01	1.407E-01	2.275E-01	2.130E-01	2.167E-01			
	1.701E-01	1.714E-01	1.404E-01	2.284E-01	2.161E-01	2.180E-01			
	1.707E-01	1.718E-01	1.406E-01	2.277E-01	2.140E-01	2.161E-01			
	1.698E-01	1.722E-01	1.407E-01	2.277E-01	2.154E-01	2.173E-01			
	1.703E-01	1.719E-01	1.408E-01	2.271E-01	2.160E-01	2.171E-01			
17,000	3.195E-01	3.214E-01	2.637E-01	4.340E-01	4.050E-01	4.150E-01			
	3.120E-01	3.226E-01	2.612E-01	4.320E-01	4.030E-01	4.080E-01			
	3.205E-01	3.206E-01	2.609E-01	4.300E-01	4.030E-01	4.080E-01			
	3.208E-01	3.219E-01	2.636E-01	4.370E-01	4.060E-01	4.090E-01			
	3.224E-01	3.224E-01	2.631E-01	4.300E-01	4.050E-01	4.100E-01			

Table XII. Voltage readings of Case L-1 for pressure drop measurement

Unit – Voltage: V

Re	V for Pressure								
	V <sub>P1</sub>	V <sub>P2</sub>	V <sub>P3</sub>	V <sub>P4</sub>	V <sub>P5</sub>	V <sub>P6</sub>	V <sub>P7</sub>	V <sub>P8</sub>	V <sub>P9</sub>
	1st pressure drop			2nd pressure drop			3rd pressure drop		
7,000	1.050E-02	1.050E-02	1.070E-02	1.290E-02	1.300E-02	1.310E-02	1.460E-02	1.470E-02	1.490E-02
	1.060E-02	1.050E-02	1.070E-02	1.290E-02	1.300E-02	1.300E-02	1.450E-02	1.470E-02	1.490E-02
	1.050E-02	1.050E-02	1.070E-02	1.300E-02	1.300E-02	1.310E-02	1.450E-02	1.470E-02	1.490E-02
	1.050E-02	1.050E-02	1.060E-02	1.290E-02	1.290E-02	1.310E-02	1.460E-02	1.470E-02	1.490E-02
	1.050E-02	1.050E-02	1.070E-02	1.290E-02	1.300E-02	1.300E-02	1.460E-02	1.470E-02	1.490E-02
12,000	1.590E-02	1.570E-02	1.610E-02	2.730E-02	2.710E-02	2.730E-02	3.340E-02	3.410E-02	3.460E-02
	1.590E-02	1.570E-02	1.610E-02	2.720E-02	2.720E-02	2.740E-02	3.360E-02	3.400E-02	3.460E-02
	1.590E-02	1.570E-02	1.610E-02	2.730E-02	2.710E-02	2.740E-02	3.340E-02	3.410E-02	3.450E-02
	1.590E-02	1.570E-02	1.610E-02	2.720E-02	2.720E-02	2.730E-02	3.350E-02	3.410E-02	3.460E-02
	1.590E-02	1.570E-02	1.610E-02	2.710E-02	2.710E-02	2.740E-02	3.360E-02	3.410E-02	3.460E-02
17,000	2.820E-02	2.800E-02	2.890E-02	5.380E-02	5.390E-02	5.420E-02	6.630E-02	6.780E-02	6.850E-02
	2.820E-02	2.800E-02	2.910E-02	5.400E-02	5.380E-02	5.430E-02	6.630E-02	6.770E-02	6.870E-02
	2.820E-02	2.790E-02	2.910E-02	5.380E-02	5.380E-02	5.430E-02	6.640E-02	6.780E-02	6.860E-02
	2.820E-02	2.800E-02	2.900E-02	5.390E-02	5.380E-02	5.430E-02	6.620E-02	6.770E-02	6.850E-02
	2.820E-02	2.790E-02	2.900E-02	5.380E-02	5.380E-02	5.430E-02	6.640E-02	6.770E-02	6.860E-02
Re	V <sub>P10</sub>	V <sub>P11</sub>	V <sub>P12</sub>	V <sub>P13</sub>	V <sub>P14</sub>	V <sub>P15</sub>			
	4th pressure drop			5th pressure drop					
7,000	1.720E-02	1.720E-02	1.740E-02	1.980E-02	2.000E-02	1.990E-02			
	1.720E-02	1.720E-02	1.740E-02	1.980E-02	1.990E-02	1.990E-02			
	1.720E-02	1.720E-02	1.730E-02	1.980E-02	1.990E-02	1.990E-02			
	1.720E-02	1.720E-02	1.740E-02	1.980E-02	1.990E-02	1.990E-02			
	1.720E-02	1.720E-02	1.730E-02	1.980E-02	1.990E-02	1.990E-02			
12,000	4.270E-02	4.270E-02	4.310E-02	5.040E-02	5.060E-02	5.080E-02			
	4.260E-02	4.260E-02	4.310E-02	5.050E-02	5.060E-02	5.090E-02			
	4.240E-02	4.270E-02	4.330E-02	5.040E-02	5.070E-02	5.060E-02			
	4.250E-02	4.270E-02	4.330E-02	5.040E-02	5.070E-02	5.050E-02			
	4.260E-02	4.250E-02	4.320E-02	5.050E-02	5.060E-02	5.070E-02			
17,000	8.530E-02	8.560E-02	8.650E-02	1.013E-01	1.017E-01	1.016E-01			
	8.530E-02	8.550E-02	8.640E-02	1.014E-01	1.019E-01	1.015E-01			
	8.540E-02	8.540E-02	8.660E-02	1.015E-01	1.017E-01	1.015E-01			
	8.530E-02	8.540E-02	8.650E-02	1.018E-01	1.016E-01	1.018E-01			
	8.520E-02	8.570E-02	8.650E-02	1.016E-01	1.015E-01	1.016E-01			

Table XIII. Voltage readings of Case L-2 for pressure drop measurement

Unit – Voltage: V

Re	V for Pressure								
	V <sub>P1</sub>	V <sub>P2</sub>	V <sub>P3</sub>	V <sub>P4</sub>	V <sub>P5</sub>	V <sub>P6</sub>	V <sub>P7</sub>	V <sub>P8</sub>	V <sub>P9</sub>
	1st pressure drop			2nd pressure drop			3rd pressure drop		
7,000	9.100E-03	9.100E-03	9.400E-03	1.230E-02	1.250E-02	1.200E-02	1.450E-02	1.420E-02	1.450E-02
	9.100E-03	9.100E-03	9.400E-03	1.230E-02	1.250E-02	1.190E-02	1.450E-02	1.410E-02	1.440E-02
	9.100E-03	9.100E-03	9.400E-03	1.230E-02	1.260E-02	1.190E-02	1.450E-02	1.420E-02	1.460E-02
	9.100E-03	9.100E-03	9.400E-03	1.230E-02	1.260E-02	1.180E-02	1.450E-02	1.420E-02	1.460E-02
	9.100E-03	9.100E-03	9.400E-03	1.230E-02	1.260E-02	1.190E-02	1.450E-02	1.420E-02	1.460E-02
12,000	1.460E-02	1.450E-02	1.550E-02	2.890E-02	2.960E-02	2.760E-02	3.690E-02	3.610E-02	3.760E-02
	1.460E-02	1.440E-02	1.560E-02	2.890E-02	2.980E-02	2.750E-02	3.700E-02	3.610E-02	3.710E-02
	1.460E-02	1.450E-02	1.550E-02	2.890E-02	2.970E-02	2.760E-02	3.720E-02	3.620E-02	3.710E-02
	1.460E-02	1.450E-02	1.550E-02	2.900E-02	2.970E-02	2.770E-02	3.730E-02	3.620E-02	3.740E-02
	1.460E-02	1.450E-02	1.560E-02	2.890E-02	2.970E-02	2.770E-02	3.690E-02	3.610E-02	3.740E-02
17,000	2.770E-02	2.710E-02	2.930E-02	5.870E-02	5.950E-02	5.530E-02	7.470E-02	7.300E-02	7.530E-02
	2.760E-02	2.710E-02	2.920E-02	5.890E-02	5.990E-02	5.520E-02	7.460E-02	7.330E-02	7.510E-02
	2.750E-02	2.700E-02	2.930E-02	5.860E-02	5.940E-02	5.540E-02	7.490E-02	7.320E-02	7.560E-02
	2.750E-02	2.690E-02	2.920E-02	5.870E-02	5.970E-02	5.540E-02	7.500E-02	7.330E-02	7.520E-02
	2.760E-02	2.700E-02	2.920E-02	5.820E-02	5.940E-02	5.550E-02	7.490E-02	7.320E-02	7.540E-02
Re	V <sub>P10</sub>	V <sub>P11</sub>	V <sub>P12</sub>	V <sub>P13</sub>	V <sub>P14</sub>	V <sub>P15</sub>			
	4th pressure drop			5th pressure drop					
7,000	1.800E-02	1.800E-02	1.730E-02	2.110E-02	2.110E-02	2.170E-02			
	1.800E-02	1.790E-02	1.740E-02	2.120E-02	2.100E-02	2.160E-02			
	1.810E-02	1.800E-02	1.740E-02	2.110E-02	2.110E-02	2.160E-02			
	1.800E-02	1.810E-02	1.740E-02	2.110E-02	2.100E-02	2.150E-02			
	1.800E-02	1.800E-02	1.730E-02	2.110E-02	2.100E-02	2.150E-02			
12,000	4.760E-02	4.780E-02	4.620E-02	5.640E-02	5.600E-02	5.760E-02			
	4.750E-02	4.770E-02	4.590E-02	5.640E-02	5.620E-02	5.760E-02			
	4.740E-02	4.760E-02	4.600E-02	5.620E-02	5.600E-02	5.770E-02			
	4.760E-02	4.760E-02	4.600E-02	5.610E-02	5.610E-02	5.770E-02			
	4.740E-02	4.720E-02	4.590E-02	5.660E-02	5.600E-02	5.770E-02			
17,000	9.670E-02	9.650E-02	9.350E-02	1.147E-01	1.140E-01	1.177E-01			
	9.680E-02	9.640E-02	9.330E-02	1.149E-01	1.145E-01	1.178E-01			
	9.670E-02	9.690E-02	9.320E-02	1.150E-01	1.142E-01	1.179E-01			
	9.680E-02	9.660E-02	9.310E-02	1.145E-01	1.139E-01	1.174E-01			
	9.690E-02	9.630E-02	9.300E-02	1.149E-01	1.140E-01	1.180E-01			

Table XIV. Voltage readings of Case L-3 for pressure drop measurement

Unit – Voltage: V

Re	V for Pressure								
	V <sub>P1</sub>	V <sub>P2</sub>	V <sub>P3</sub>	V <sub>P4</sub>	V <sub>P5</sub>	V <sub>P6</sub>	V <sub>P7</sub>	V <sub>P8</sub>	V <sub>P9</sub>
	1st pressure drop			2nd pressure drop			3rd pressure drop		
7,000	9.700E-03	9.600E-03	1.020E-02	1.520E-02	1.600E-02	1.250E-02	1.660E-02	1.600E-02	1.950E-02
	9.700E-03	9.700E-03	1.020E-02	1.510E-02	1.610E-02	1.240E-02	1.650E-02	1.600E-02	1.940E-02
	9.700E-03	9.600E-03	1.030E-02	1.530E-02	1.600E-02	1.240E-02	1.680E-02	1.590E-02	1.950E-02
	9.700E-03	9.600E-03	1.020E-02	1.500E-02	1.600E-02	1.240E-02	1.650E-02	1.590E-02	1.950E-02
	9.700E-03	9.600E-03	1.030E-02	1.510E-02	1.600E-02	1.240E-02	1.670E-02	1.600E-02	1.940E-02
12,000	1.490E-02	1.420E-02	1.660E-02	3.700E-02	3.960E-02	2.730E-02	4.070E-02	3.960E-02	4.970E-02
	1.480E-02	1.430E-02	1.650E-02	3.710E-02	3.950E-02	2.700E-02	4.090E-02	3.970E-02	4.930E-02
	1.490E-02	1.430E-02	1.660E-02	3.690E-02	3.910E-02	2.710E-02	4.110E-02	3.950E-02	4.930E-02
	1.490E-02	1.430E-02	1.650E-02	3.700E-02	3.980E-02	2.710E-02	4.120E-02	3.920E-02	4.960E-02
	1.490E-02	1.430E-02	1.650E-02	3.770E-02	3.960E-02	2.720E-02	4.090E-02	3.910E-02	4.950E-02
17,000	2.740E-02	2.630E-02	3.110E-02	7.550E-02	7.900E-02	5.470E-02	8.270E-02	7.900E-02	9.930E-02
	2.760E-02	2.630E-02	3.120E-02	7.570E-02	8.040E-02	5.510E-02	8.240E-02	7.940E-02	1.002E-01
	2.740E-02	2.630E-02	3.120E-02	7.500E-02	7.950E-02	5.480E-02	8.340E-02	7.920E-02	1.005E-01
	2.730E-02	2.620E-02	3.130E-02	7.520E-02	7.950E-02	5.490E-02	8.270E-02	7.910E-02	1.009E-01
	2.750E-02	2.630E-02	3.120E-02	7.560E-02	7.960E-02	5.500E-02	8.260E-02	7.900E-02	1.008E-01
Re	V <sub>P10</sub>	V <sub>P11</sub>	V <sub>P12</sub>	V <sub>P13</sub>	V <sub>P14</sub>	V <sub>P15</sub>			
	4th pressure drop			5th pressure drop					
7,000	2.220E-02	2.230E-02	2.010E-02	2.530E-02	2.480E-02	2.650E-02			
	2.200E-02	2.220E-02	1.990E-02	2.550E-02	2.470E-02	2.670E-02			
	2.200E-02	2.240E-02	1.990E-02	2.560E-02	2.470E-02	2.670E-02			
	2.230E-02	2.220E-02	1.990E-02	2.550E-02	2.480E-02	2.700E-02			
	2.210E-02	2.210E-02	1.980E-02	2.540E-02	2.480E-02	2.690E-02			
12,000	5.690E-02	5.810E-02	5.170E-02	6.710E-02	6.500E-02	7.060E-02			
	5.660E-02	5.780E-02	5.200E-02	6.700E-02	6.490E-02	7.020E-02			
	5.650E-02	5.820E-02	5.180E-02	6.660E-02	6.470E-02	7.040E-02			
	5.710E-02	5.790E-02	5.150E-02	6.660E-02	6.440E-02	7.020E-02			
	5.710E-02	5.790E-02	5.160E-02	6.650E-02	6.480E-02	7.060E-02			
17,000	1.146E-01	1.162E-01	1.036E-01	1.350E-01	1.309E-01	1.441E-01			
	1.156E-01	1.172E-01	1.036E-01	1.355E-01	1.319E-01	1.432E-01			
	1.150E-01	1.166E-01	1.039E-01	1.360E-01	1.317E-01	1.436E-01			
	1.149E-01	1.172E-01	1.040E-01	1.362E-01	1.318E-01	1.442E-01			
	1.149E-01	1.164E-01	1.033E-01	1.362E-01	1.324E-01	1.429E-01			

Table XV. Ambient, orifice, and inlet temperature measurement

Re	Case S-1			Case S-2			Case S-3		
	T <sub>ambient</sub> [K]	T <sub>orifice</sub> [K]	T <sub>inlet</sub> [K]	T <sub>ambient</sub> [K]	T <sub>orifice</sub> [K]	T <sub>inlet</sub> [K]	T <sub>ambient</sub> [K]	T <sub>orifice</sub> [K]	T <sub>inlet</sub> [K]
7,000	2.98E+02	3.00E+02	2.97E+02	2.98E+02	3.00E+02	2.98E+02	2.95E+02	2.97E+02	2.95E+02
12,000	2.98E+02	3.00E+02	2.98E+02	2.98E+02	3.00E+02	2.97E+02	2.95E+02	2.98E+02	2.95E+02
17,000	2.98E+02	3.00E+02	2.98E+02	2.97E+02	2.99E+02	2.97E+02	2.97E+02	2.99E+02	2.97E+02
Re	Case L-1			Case L-2			Case L-3		
	T <sub>ambient</sub> [K]	T <sub>orifice</sub> [K]	T <sub>inlet</sub> [K]	T <sub>ambient</sub> [K]	T <sub>orifice</sub> [K]	T <sub>inlet</sub> [K]	T <sub>ambient</sub> [K]	T <sub>orifice</sub> [K]	T <sub>inlet</sub> [K]
7,000	2.97E+02	2.98E+02	2.97E+02	2.98E+02	2.99E+02	2.97E+02	2.98E+02	2.99E+02	2.98E+02
12,000	2.97E+02	2.99E+02	2.97E+02	2.98E+02	2.99E+02	2.97E+02	2.98E+02	2.99E+02	2.97E+02
17,000	2.97E+02	2.98E+02	2.97E+02	2.98E+02	2.99E+02	2.98E+02	2.98E+02	2.99E+02	2.98E+02

Table XVI. Voltage and current readings for segmented walls heat loss measurement

Unit – Voltage: V, Current I: A

V			I		
1st plate	2nd plate	3rd plate	1st plate	2nd plate	3rd plate
1.27E+01	1.06E+01	1.29E+01	2.08E-01	1.89E-01	2.27E-01
1.27E+01	1.06E+01	1.29E+01	2.08E-01	1.89E-01	2.27E-01
1.27E+01	1.06E+01	1.29E+01	2.08E-01	1.89E-01	2.27E-01
1.27E+01	1.06E+01	1.29E+01	2.08E-01	1.89E-01	2.27E-01
1.27E+01	1.06E+01	1.29E+01	2.08E-01	1.89E-01	2.27E-01



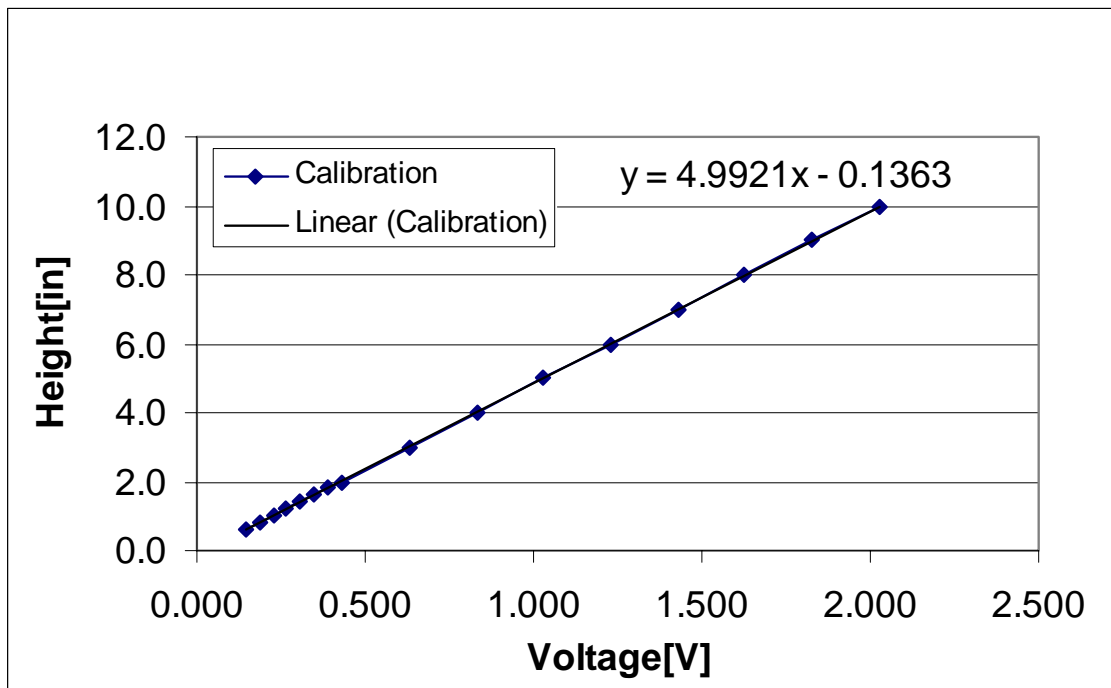


Fig. 9. Pressure transducer calibration result.

## VITA

Yonghee Lee

Education:

B.S. Machine Design, Sungkyunkwan University, Seoul, 1998

Permanent Address:

977-17, Young-sin Ga-dong 206-Ho, Doksan-3-Dong, 153-013, Seoul, Korea

The typist for this thesis was Yonghee Lee.